Leveraging single-cell transcriptomics of developing rat ocular outflow tissues to prioritize congenital glaucoma candidate genes

Sean M. Martin[1¶], Kristina N. Whisenhunt[1¶], Stuart W. Tompson[1,2*]

[1] Department of Ophthalmology and Visual Sciences, School of Medicine and Public Health, University of Wisconsin, Madison, Wisconsin, USA.

[2] McPherson Eye Research Institute, University of Wisconsin, Madison, Wisconsin, USA.

[*]Corresponding author

Email: stuarttompson7@gmail.com (ST)

ORCID identifier (ST): https://orcid.org/0000-0001-9788-6730

[¶]These authors contributed equally to this work.

Commercial relationships disclosures: The authors declare no competing interest.

Abstract

Primary congenital glaucoma (PCG) is a severe, early-onset eye disease most often caused by abnormal development of the aqueous humor outflow pathway (AHOP). Located circumferentially at the anterior chamber angle where the iris meets the cornea, the AHOP comprises the trabecular meshwork (TM) and Schlemm's canal (SC), which together regulate intraocular fluid drainage. Malformation of this pathway leads to elevated intraocular pressure, painful ocular enlargement, and retinal damage that can result in blindness. While single-gene mutations account for approximately 25% of PCG cases across diverse populations, most molecular causes remain unknown and are likely due to rare or complex genetic factors. Progress in identifying these mechanisms has been limited by a lack of detailed gene expression data during AHOP development. To address this gap, we generated the first single-cell RNA sequencing dataset from developing AHOP tissue, using rat eyes at three key stages of TM and SC formation. This high-resolution dataset contains the transcriptomic profiles of 29,626 genes across 86,653 cells clustered into 13 general cell types, which included over 10,000 cells related to TM/SC subtypes. Analysis of 44 genes previously linked to Mendelian childhood glaucoma showed that 36 (82%) were expressed in these TM/SC-related populations, validating the dataset's relevance. Notably, this study identified 395 genes selectively upregulated in developing TM/SC subtypes, revealing numerous candidates potentially involved in the formation and function of TM/SC structures. This resource will support the discovery of rare Mendelian disease genes and inform the development of polygenic risk scores for complex genetics underlying early-onset forms of glaucoma.

Introduction

In the eye, aqueous humor (AH) is a clear fluid produced by the ciliary body that flows through the anterior chamber, delivering nutrients, clearing metabolic waste, and helping maintain ocular shape for

38 focused vision. AH production is balanced via drainage through structures located at the interface
39 between the cornea and iris – the conventional AH outflow pathway (AHOP). To prevent excess
40 intraocular pressure (IOP), fluid exits the eye through the trabecular meshwork (TM) and Schlemm's
41 canal (SC), which connects to the systemic blood circulatory system via collector channels (Fig 1).
42 Failure to correctly develop these intricate outflow structures can lead to elevated eye pressure, damage
43 to retinal ganglion cells and the optic nerve, and early-onset vision loss known as primary congenital
44 glaucoma.

45 The molecular mechanisms of primary congenital glaucoma have been elucidated in only 25% of cases,
46 and all involved genes critical for the proper formation and function of the TM and/or SC tissues.[1-4] Our
47 understanding of genes important for AHOP development has been restricted by the limited availability
48 and complex heterogeneity of these early tissues. Several studies have recently employed single-cell
49 RNA sequencing (scRNAseq) to catalogue gene expression in outflow tissues from humans, nonhuman
50 primates, pigs and mice,[5-9] but all profiled mature tissues. To date, no study has attempted to identify the
51 cells and molecular pathways active during the early development and growth of the TM and/or SC
52 tissues relevant to the etiology of congenital glaucoma.

53 The mature TM is a sieve-like structure composed of three distinct layers, each contributing to the
54 regulation of AH outflow and IOP.[10] AH first passes through the uveal meshwork – a loose, open
55 network of connective tissue encased in a continuous basement membrane and lined with endothelial-
56 like TM cells (TMCs). This layer serves to filter larger cellular debris and neutralizes reactive oxygen
57 species (ROS). The middle corneoscleral layer consists of TMC-covered collagen and elastin-rich beams
58 with smaller pores for finer filtration and additional ROS scavenging. Finally, the juxtacanalicular tissue
59 (JCT), composed of loosely arranged extracellular matrix (ECM) and star-shaped fibroblast-like TMCs,
60 regulates AH outflow resistance in coordination with the inner wall of SC.[11] The mature SC is composed

61 of a monolayer of vascular endothelial cells that share molecular characteristics with blood and
62 lymphatic endothelial cells.[12,13] The SC endothelial cells (SECs) can be divided into inner-wall (IW)
63 cells that lay against the TM and outer-wall (OW) cells located towards the outside of the eye. The IW
64 allows AH outflow through giant vacuoles and pores whilst maintaining a blood-aqueous barrier,
65 whereas the OW maintains the canal's structure and passes AH into collector channels that lead away
66 from the eye.[14]

67 Here, we present a study utilizing scRNAseq to identify the major cell types and their associated gene
68 expression profiles during three major stages of SC and TM development in rats. Rat tissues share all
69 major stages of anterior chamber angle development and morphological characteristics of the AHOP
70 with humans, and they also enable acquisition of larger quantities of relevant tissue components versus
71 mice. Remé and colleagues performed detailed electron and light microscopy studies of rat AHOP
72 development,[15] observing AHOP anlage formation at embryonic day 7. By postnatal day 5 (P5), the
73 presumptive TM remained an undifferentiated condensation of periocular mesenchyme (POM), and a
74 rudimentary cluster of blood vessels that would become SC were visible. Between P5 and P10, sheets of
75 primitive TM formed, and the young SC vessels became enlarged. Between P10 and P20, the TM
76 became five or six layers with distinct cells and SC had fused into a vessel with a single vacuole. The
77 final structures were formed between P20 and P60, when the TM became less dense with the formation
78 of Fontana's spaces and beams, and both the TM and SC elongated into their mature forms. Based on
79 these developmental observations, we profiled these specialized tissues at P7-9, P14-16, and P27-29.

80

Results

Limbal cell acquisition

Histological examination of rat AHOP tissues at P8, P15, and P28 confirmed the morphological findings described by Remé and colleagues (Fig 2).[15] In total, three male and three female limbal tissue strips (region highlighted in Fig 1) were dissected and dissociated into single-cell suspensions at each of the three developmental ages. Samples contained all cell types located between the cornea and sclera on the exterior surface of the eye to the ciliary body on the inner side. The final dataset contained transcriptomic profiles of 29,626 genes from 86,653 limbal cells, visualized as 13 major cell type clusters (C0-C12) according to overall gene expression similarity (Fig 2). The contributions of cells from the 18 tissue samples to each cluster are provided in S1 Table. The major cell type identities within these clusters were revealed through differential expression of published marker genes, as described in Supporting Information ("Identification of major limbal cell types" in S1 Appendix and Fig S1).

Vascular endothelium and the identification of Schlemm's canal cells

Vascular endothelial cells (VECs), including those that form Schlemm's canal (SECs), uniquely express *Pecam1* and formed a single independent cluster (C8, Fig S2). To specifically identify SECs, these 3,155 cells were reclustered into nine subtypes (VEC0-VEC8, Fig 3 and Fig S3). Their vascular identities were ascertained through interrogation of differentially expressed genes, as described in Supporting Information ("Identification of VEC subtypes" in S1 Appendix and Fig S3). In mice, SECs share transcriptional features of both blood and lymphatic endothelia, expressing *Cd34* and *Prox1*, but not *Pdpn* or *Vwf*, yet they also retain distinct gene expression patterns that reflect their specialized role in AH drainage.[9,12,13,16] SECs expressing these hybrid features formed VEC1 and a subpopulation of VEC7

102 (Fig 3 and Fig S3). Consistent with the growth and maturation of SC, the SECs population (VEC1)
103 dramatically increased with sample age (Fig 3 and Fig S4). The two distinct SEC-related populations in
104 VEC7 were formed from proliferating cells highly expressing *Top2a* and *Mki67*.[17,18] These populations
105 also changed in size with tissue age (Fig S4). As SC developed, the larger population displaying a
106 stronger blood vessel-like profile (high *Flt1*, *Lrg1*, *Stc1*, *Sema3e*, *Tcf15*, low *Prox1*) reduced in number,
107 whilst the smaller island exhibiting more SEC-like expression became numerous. This was consistent
108 with cells involved in the formation of SC - proliferating VECs shifting their expression profile during
109 canalogenesis from blood vessel-like to a more hybrid-lymphatic phenotype and ultimately contributing
110 to the more specialized SEC pool in VEC1.[12]

111 In mouse studies, SECs do not significantly express the *Lyve1* gene, which is restricted to lymphatic
112 vessels and a subset of interstitial macrophages that preferentially localize near vessels.[9,12,13,16,19] In
113 contrast, our studies in rat have revealed *Lyve1* expression not only in lymphatic vessels and interstitial
114 macrophages but also at low levels in more mature SECs (Fig 3). We confirmed this finding at the
115 protein level, immunostaining whole mounted tissues for Pecam1 to visualize SC, Aif1 to broadly
116 highlight macrophages, and Lyve1 (Fig 3).[20] At P4, areas of SC consisted of rudimentary smaller vessels
117 that did not express Lyve1, and could be observed undergoing macrophage-aided vessel fusion (arrow).
118 At P7, regions of SC comprised clustered vessels that were not fully fused and Lyve1 levels remained
119 insignificant. At P14, Lyve1 expression by SECs was distinct from resident macrophages and was
120 stronger towards the inner wall. At P28, Lyve1 expression by SECs was strongest and remained
121 primarily towards the inner wall, reflecting the acquisition of lymphatic-like properties by the mature
122 outflow vessel.

123

Identification of SEC subtypes

In total, 655 VECs with SC-like profiles were identified, comprising 109 actively proliferating cells and 546 that were quiescent and more specialized. To resolve further SEC heterogeneity, VEC1 and VEC7 cells were isolated and re-clustered, yielding six subpopulations with distinct gene expression profiles (SEC0-SEC5, Fig 4; heatmap of top differentially expressed genes between SEC clusters provided in Fig S5). To support this dataset, *in situ* hybridization (ISH) studies were performed on AHOP tissues to confirm the localized expression of key SEC markers (Fig S6). The method used fluorescent probes to detect individual mRNA transcripts in and around cell nuclei in intact but thin tissue sections. Due to the limited number of nuclei captured from sections across the lumen of SC, this technique was only able to effectively localize robustly expressed genes. Furthermore, as observed for *Pecam1*, *Tek*, *Flt1*, and *Cd34*, transcripts were more readily detected in IW versus OW cells, despite their well-established expression throughout SC (Fig S6).

SECs derived from VEC1 formed four subclusters, while SECs from VEC7 remained in two spatially isolated populations (SEC3 and SEC5) distinguished by strong expression of genes related to cell replication. SEC3 cells were most abundant during early SC development (P7) and expressed genes associated with angiogenic sprouting and proliferation, including *Top2a*, *Mki67*, *Car8*, *Enpp2*, and *Nostrin*.[17,18,21-23] In contrast, SEC5 cells lacked sprouting markers but expressed genes for lymphatic processes (*Prox1*, *Lyve1*, and *Nfatc1*,[24]) and vessel remodeling (*Sema3a*[25], *Sema3d*[26]). ISH studies of *Top2a* expression were unable to localize SEC3/SEC5 cells to a specific SC region (Fig S6), which reflected their limited population at any age.

SEC2 cells were observed during mid-stage development of SC and displayed transcriptional features similar to SEC5 but without proliferation markers. Specifically upregulated expression was related to

progenitor/stem cell identity (*Mast4*,[27] *Kit*[28]), leukocyte chemotaxis (*Sele*,[29]), motility (*Sh3pxd2b*[30]), ECM modification (*Adamts17*[31]), and angiogenesis regulation (*Nox4*,[32] *Vash1*[33]). The expression of *Sele* has previously been attributed to OW cells in adult mice.[9] ISH studies of *Sele* expression in whole tissues reflected the scRNAseq data, with transcripts more readily detected later in SC development, but the signal was too limited to confirm localization to a specific region such as the OW (Fig S6). Conversely, *Nox4* expression signal was strong throughout AHOP development in both the IW and OW at P7 and P14 but appeared more restricted to the IW at P31 (Fig S6).

The largest late-stage populations of SEC0 and SEC1 cells showed closely related profiles, including expression of a gap junction protein associated with lymphatic-like endothelia, *Gjc2*.[34] ISH studies of *Gjc2* localized the most robust expression to IW cells at P14 (Fig S6). Specifically, SEC0 cells showed the strongest expression of *Gjc2* and *Hspb1*, a protein involved in endothelial movement.[35] Conversely, SEC1 cells exhibited enhanced expression related to lymphatic identity (*Prox1*, *Lyve1*, *Nfatc1*), vessel remodeling (*Sema3a*, *Sema3d*), regulation of angiogenesis (*Skil*[36], *Pgf*[37]), ECM remodeling (*Thsd4*[38]), and a chemokine that attracts immune cells toward lymphatic-like vessels (*Ccl21*[39,40]). High *Prox1* and *Ccl21* expression have previously been associated with IW cells in adult mice.[9] Consistent with this, ISH studies of *Ccl21* identified low expression localized to the IW (Fig S6). Furthermore, SEC1 cells also expressed genes that could be related to IW function, such as flow–responsive lymphatic remodeling (*Dtx1*[41,42]), lumen maintenance (*Sh3gl3*[43]), and sodium transport (*Scn5a*[44]). The smallest late-stage population of SEC4 cells were enriched for genes involved in integrin signaling (*Postn*[45]), cytoskeletal dynamics (*Wipf3*[46]), vascular integrity (*Plxna4*[47]), and maintenance of vascular homeostasis (*Nos1*[48]). Like SEC2, SEC4 cells also expressed *Sele*, which suggested they were derived from the OW.

While enhanced expression of the ECM component nephronectin (*Npnt*[49]) has been reported for a subset of IW cells in adult mice,[9] this gene was more broadly expressed in all rat SECs with particular

169 enrichment in SEC4 (putative OW cells). Interestingly, both SEC1 (IW) and SEC4 (OW) cells shared
170 expression of two genes previously identified in human lymphatics, *Mmrn1* and *Pkhd1l1*.[50] Finally,
171 most SEC clusters selectively expressed a subunit of the sodium/potassium ATPase pump that is critical
172 for cell volume maintenance (*Fxyd2*).[51] Given that *Fxyd2* expression in the rat limbus was otherwise
173 restricted to monocytes, this gene emerged as one of the most specific markers for all SEC types in our
174 dataset.

175 Identification of trabecular meshwork cells within fibroblast-like 176 populations

177 As demonstrated by Remé et al., in rats the TM begins forming as a condensed mass of multipotent
178 periocular mesenchyme (POM) between P7-P9, which differentiates into primitive TM sheets.[15] These
179 early POM cells express high levels of the developmental transcription factor *Pitx2*,[52] which is
180 subsequently downregulated as they transition into TM cells (TMCs) - elongating, flattening, and
181 becoming separated by extracellular fibers that organize into lamellae and connective tissue.[53] By P14-
182 P16 the layered TM structures are evident, and by P27-P29 the tissue resembles mature architecture with
183 a meshwork of beams and large Fontana's spaces.[15]

184 In the mature tissue, TMCs across all three layers express shared genes, including *Col4a1* and *Col8a1*
185 (Type IV and VIII collagen alpha chains),[11] *Eln* (elastin),[54] *Nid1* (nidogen-1),[11] *Myoc* (myocilin),[7] *Mgp*
186 and *Spp1* (calcification inhibitors),[55,56] *Angpt1* and *Svep1* (angiogenic mediators),[8,57] and *Ltbp2* (an ECM
187 protein involved in TGF-β regulation).[58] TMCs also express *Acta2* (smooth muscle actin),[59] but not *Des*
188 (desmin),[11] distinguishing them from smooth muscle cells. Unlike the adjacent corneal endothelia,
189 TMCs do not express *Col4a3*, encoding the α3 chain of type IV collagen.[11]

190 Layer-specific functions of TMCs are reflected by their differential gene expression. TMCs of the uveal
191 and corneoscleral layers secrete tissue plasminogen activator (*Plat*) to maintain pathway patency,[60]
192 superoxide dismutases (*Sod1*, *Sod2*, *Sod3*) to combat reactive oxygen species (ROS),[61] and *Il6* for IOP
193 regulation.[62] In primates, hyaluronic acid (HA) is present in the JCT ECM but it is not synthesized
194 locally.[63] Instead, HA is produced by *Has1/2/3* in uveal and corneoscleral TMCs[63,64] and is carried into
195 the JCT by AH flow.[59] JCT-resident TMCs are identifiable by elevated expression of chondroadherin
196 (*Chad*),[5] tenascin-C (*Tnc*),[65] angiopoietin-like 7 (*Angptl7*),[5-7] chitinase-3-like protein 1 (*Chi3l1*),[5]
197 thrombospondin-1 (*Thbs1*),[66] and crystallin alpha B (*Cryab*).[11,67]

198 To identify TMCs in the rat limbal dataset, cells were screened for high expression of the POM marker
199 *Pitx2*, along with four genes previously localized to the TM: *Myoc*, *Angpt1*, *Svep1*, and *Ltbp2*.[7,8,58] These
200 genes showed variable expression across several limbal clusters but all were strongly enriched in C1
201 (Fig 5). Consequently, subsequent analyses were focused on this population of 21,735 fibroblast-like
202 cells.

203 C1 cells were isolated and reclustered into four fibroblast-like (FBL0-FBL3) subtypes (Fig S7), and
204 their identities inferred from established marker genes, as described in Supporting Information
205 ("Identification of fibroblast-like subtypes" in S1 Appendix and Fig S7; heatmap of top differentially
206 expressed genes between FBL clusters provided in Fig S8). Putative TMC-like cells were identified
207 within FBL0, isolated, and the 10,037 cells re-clustered into seven groups (TMC0-TMC6, Fig 6;
208 heatmap of top differentially expressed genes between TMC clusters provided in Fig S9). The TMC
209 cluster data correlated with ISH studies in tissue sections, which showed expression of the pan-TM
210 marker *Myoc* increased progressively with tissue maturation, starting posterior to the rudimentary SC
211 and spreading throughout the TM as it developed (Fig S10). Conversely the *Cyp1b1* gene, in which

212 mutations account for most cases of primary congenital glaucoma, was expressed more highly in P7 and
213 P14 TMCs than at P31 (Fig S11).

214 To investigate the developmental trajectory of these subpopulations, we analyzed changes in cell
215 abundance across developmental timepoints. Cell populations in TMC1, TMC2, and TMC4 decreased
216 over time, suggesting they represent progenitor or transitional states (Fig 6). Notably, TMC2 cells
217 exhibited a marked shift in UMAP position, indicating broad changes in expression profile as the TM
218 developed. TMC5 cells largely maintained their numbers, while TMC6 cells gradually expanded - both
219 accompanied by dynamic changes in gene expression. In contrast, TMC0 and TMC3 expanded
220 significantly during mid-to-late developmental stages, which implicated them as terminally
221 differentiated TMCs. Minimal expression of proliferation (*Mki67*, *Top2a*) and apoptosis (*Casp3*,
222 *Casp7*[68]) markers suggested cell state differentiation as the major cause of the cluster changes.

223 The largest terminal cluster, TMC0, showed the strongest *Myoc* expression but contained few cells at P7
224 (Fig 6). This population expanded substantially over time and expressed hallmark markers of the JCT,
225 including *Chad*, *Angptl7*, *Chi3l1*, and *Thbs1*.[66] Additional genes enriched in TMC0 cells included
226 *Pla2g2a*, *Shisa3*, *Ccn5*, *Cilp2*, *Podnl1*, and *Nrgn*. ISH studies of *Chad* detected strong expression in
227 corneal and limbal stroma and confirmed weaker expression within a subset of the TM that localized
228 more closely to the JCT at P31 (Fig S12).

229 The second and third largest terminal clusters, TMC3 and TMC6, expressed key markers of the uveal
230 and corneoscleral TM layers, including *Plat* (tissue-type plasminogen activator), *Il6* (interleukin-6), and
231 *Sod2* (superoxide dismutase 2).[60-62] The clusters also expressed *Vcan* (versican), which binds HA to
232 form large proteoglycan aggregates and plays a role in modulating AH outflow resistance in the JCT[69,70],
233 and the metalloprotease *Adamts1*, which cleaves versican into its bioactive form.[71] These data suggest
234 that, like HA, versican is secreted by uveal and corneoscleral TMCs and transported into the JCT by

235 aqueous flow.[63] TMC3 and TMC6 cells also expressed *Gsn*, *Ctsc*, *Heyl*, and the TM lamellae-associated
236 type V collagen (*Col5a3*[72]). ISH studies of *Gsn* detected moderate expression widely throughout the P7
237 and P14 tissues which became strongly enriched in the TM layers by P31 (Fig S13). Specifically, TMC3
238 cells could be distinguished by selective expression of *Apoe*, *Nav3*, *Crlf1*, *Csmd1*, and *Pdlim3*. ISH
239 studies of *Apoe* confirmed selective expression within a subset of the TM (Fig S14). Conversely, TMC6
240 cells uniquely expressed HA synthase (*Has1*),[63,64] TM-associated mechanosensitive ion channel
241 (*Piezo2*),[73] *Clec3b*, *Sema3d*, *Pi16*, *Ccl11*, *Edn3*, *Gsta1*, *Enpp3*, *Enpp1*, and *Ccl7*. ISH studies for *Clec3b*
242 confirmed expression localized to a specific subset of the TM at P14 and P31 (Fig S15).

243 Significant TMC2 and TMC5 cell populations were present at all three developmental ages with subtle
244 changes in cluster locations noted, reflecting overall gene expression shifts. TMC2 cells shared a similar
245 profile to TMC0, that included JCT-like *Chad* and *Angptl7* expression, but with higher levels of *Fos* and
246 *Egr1*. ISH studies of *Fos* localized specific expression to the posterior region of the TM at P7 and P14
247 that was adjacent to SC by P31 (Fig S16). In contrast, TMC5 cells displayed a transcriptional profile that
248 included strong tendon (*Tnmd*[74]) and smooth muscle (*Acta2*, *Tagln*, *Myl9*, *Eln*) markers, as well as
249 unique expression of *Grid2* and *Cit*. ISH studies of *Tnmd* detected highly specific expression throughout
250 the TM at P7 and P14 that extended to adjacent stromal fibroblasts by P31 (Fig S17).

251 Finally, the two early-stage TM populations (TMC1 and TMC4) were significantly reduced by P28,
252 which was consistent with progenitor cells contributing to TM formation. Both clusters expressed high
253 levels of *Chad* and *Angptl7*, supporting their identity as JCT progenitors. Other genes expressed by
254 TMC0/JCT cells were also detected at higher levels in TMC1 cells, such as *Igfbp2*, *Pdgfrl*, *Col8a1*, and
255 *Nrgn*. ISH studies of *Igfbp2* confirmed strong expression throughout the early TM at P7 that persisted at
256 P31 (Fig S18). Early stage TMC1 cells also shared expression of *Dlk1* with the later TMC2 and TMC5
257 cell types. Conversely, TMC4 cells were marked by higher levels of *Tgfbi*, a protein important for cell-

258 ECM interactions,[75] which ISH studies confirmed peak expression at P14 in TMCs located between SC
259 and the ciliary body (Fig S19).

260 Selective gene expression in SECs and TMCs

261 In total, this study identified 655 SC- and 10,037 TM-related cells that could be further subdivided into
262 13 distinct populations according to their distinguishing gene expression profiles. To recognize
263 molecular pathways important for the development and function of SC and the TM, differential
264 expression analyses were performed to identify genes with enhanced expression in these important cell
265 types versus all other limbal cells. For the four main SEC subtypes (SEC0, SEC1, SEC2, and SEC4),
266 244 genes with human orthologs were selectively expressed in one or more of the subclusters. Genes
267 selectively expressed by the proliferating BEC population (SEC3) were not included as these cells could
268 not be definitively related to SC versus other developing blood vessels. Only *Hoxd8*, a transcription
269 factor important for the differentiation of BECs into lymphatic-like endothelial cells,[76] was selectively
270 expressed in the proliferating SEC population (SEC5) compared to SEC3 cells. Its inclusion brought the
271 total number of selectively upregulated SEC genes to 245. In total for all seven TMC subtypes, 153
272 genes with human orthologs were selectively upregulated in one or more of the subclusters. Three genes,
273 *Ephb1*, *Lbp*, and *Sema3d*, were identified in subtypes of SECs and TMCs. Combined, this study
274 identified 395 genes selectively upregulated in cell types associated with these two critical developing
275 outflow pathway tissues (Fig 7).

276 Gene expression associated with Mendelian disease

277 We sought to assess whether genes already associated with Mendelian forms of congenital glaucoma are
278 expressed within our developing SC/TM dataset. Primary congenital glaucoma falls within a larger
279 group of congenital glaucomas that includes syndromic forms encompassing non-ocular organ systems

280 and developmental anomalies collectively referred to as anterior segment dysgenesis (ASD; OMIM
281 107250). ASD shows vast phenotypic variability of abnormalities affecting the iris, cornea, lens, TM,
282 and SC,[77] and are caused by mutations in many genes including *PAX6*, *FOXC1*, *PITX2*, *FOXE3*, *PITX3*,
283 *PXDN*, *CPAMD8*, *B3GLCT*, and *COL4A1*.[77-79] It can be difficult to diagnostically separate cases of
284 primary congenital glaucoma from the other disorders when the clinical features outside of the drainage
285 tissues are mild.[78,79] Together, this study interrogated 44/45 genes previously associated with congenital
286 glaucoma. One gene, *Guca1c*, could not be assessed in our data due to the lack of a rat ortholog. The
287 data revealed 36/44 (82%) genes were expressed by at least one SC- or TM-related cell cluster (Fig 8).

288 Gene expression associated with complex disease

289 Genome-wide association studies (GWAS) have implicated hundreds of genes in the pathogenesis of
290 glaucoma. Primary open-angle glaucoma (POAG), the leading cause of irreversible blindness
291 worldwide, is characterized by late-onset optic nerve damage, progressive visual field loss, and typically
292 elevated IOP despite open access of AH to the drainage tissues.[80,81] In 2021, Gharahkhani et al. reported
293 a multi-ethnic meta-analysis of GWAS data from 34,179 POAG cases and 349,321 controls, and
294 identified 127 risk loci that collectively explained 9.4% of familial risk.[82] Of these, 89/123 loci with
295 available IOP data were significantly associated with IOP, which suggested shared genetic etiology.
296 More recently, Han et al. (2023) reported the largest multitrait gene-based GWAS analysis (MTAG),
297 which identified 355 genes significantly associated with POAG risk.[83]

298 Given the expected role of AHOP dysfunction in POAG, we examined the expression of these POAG-
299 associated genes in our dataset. Genes were filtered to remove duplicates between the two GWAS lists,
300 those without known protein-coding rat orthologs, or those lacking expression in our scRNAseq data. In
301 cases where multiple protein-coding genes mapped to a single locus, all were included in the

assessment. Together, 372 POAG-associated genes were interrogated across SC/TM-related cell clusters (Fig S20). Many of the genes demonstrated high expression in SECs and/or TMCs, but few were selectively expressed in just those cells versus other limbal cell types. Thirteen genes were selectively expressed at substantial levels by SECs, which were *Adam15*, *Cav1*, *Cav2*, *Clic5*, *Cttnbp2*, *Egln3*, *Emid1*, *Fam53b*, *Kctd20*, *Maff*, *Pthlh*, *Tes*, and *Thsd7a*. Fourteen genes were selectively expressed at robust levels by TMCs, which were *Angpt1*, *Col24a1*, *Efemp2*, *Itgb5*, *Ltbp1*, *Ltbp2*, *Ltbp3*, *Myoc*, *Nucb2*, *Pitx2*, *Rora*, *Svep1*, *Tcf7l2*, and *Tgfb3*. Two genes, *Pde7b* and *Plce1*, were selectively enriched at in populations of both SECs and TMCs.

Discussion

This work has demonstrated the feasibility of the scRNAseq approach to broadly catalogue cell types and their associated gene expression profiles in the diminutive and complex tissues of the developing rat AHOP. This method has identified 655 VECs related to SC development, including 109 actively proliferating and 546 quiescent, as well as 10,037 cells related to the development of the TM. ISH studies reinforced the localization of these cell types to the TM/SC. Further refinement to specific regions, implicated by known marker gene expression, was restricted by the limited rat tissue size and low nuclear transcript signals obtained from thin ISH sections. As antibodies proven for rat protein detection become available, further whole tissue staining studies will enable a more detailed investigation.

Interrogation of 44 genes linked with Mendelian forms of congenital glaucoma revealed 36/44 (82%) were expressed by at least one SC- or TM-related cell cluster, validating the dataset's relevance. The classification of cell types presented here is consistent with published studies such as the expression of *Angpt1*, *Angptl7*, *Cyp1b1*, *Ltbp2*, *Myoc*, *Piezo1*, *Pitx2*, *Svep1*, and *Thbs1* in the TM,[3,5-8,57,58,66,84,85] and

324 *Col4a1*, *Piezo2*, *Tek*, and *Tie1* in SC.[2,12,73,86] Furthermore, for the eight genes which lacked TM/SC
325 cluster expression, published findings describe expression and disease mechanisms that involve tissues
326 outside of the AHOP or function during earlier developmental processes. Specifically, *CPAMD8* variants
327 cause congenital glaucoma with anterior segment dysgenesis, myopia, and ectopia lentis, likely due to
328 abnormal iris or lens morphology rather than SC/TM defects.[79,87] *CRYBB2*, associated with congenital
329 cataracts and glaucoma, is expressed in lens epithelial cells and retinal neurons, and directly prevents
330 RGC loss.[88-90] *FOXE3* and *PITX3*, both involved in early lens development, are linked to anterior
331 segment dysgenesis, with lens-cornea or iris-lens adhesions obstructing aqueous outflow.[91-93] *PRSS56*
332 mutations cause posterior microphthalmia, leading to angle-closure glaucoma due to a shallow anterior
333 chamber.[94] *MAB21L1* mutations, associated with syndromic and ocular abnormalities including
334 buphthalmos, impair anterior segment architecture in zebrafish, reducing outflow via fibrous masses
335 between the lens and cornea.[95-98] *PAX6* is essential for early differentiation of periocular mesenchyme,
336 and its loss in mice leads to an undeveloped TM and absent SC – events occurring too early in
337 development (P0-P4) to be captured in this study.[99-101] Similarly, *GPATCH3* is implicated in congenital
338 glaucoma, but its expression has only been observed in early zebrafish periocular mesenchyme and
339 corneal endothelium.[102]

340 Unexpectedly, our studies revealed expression of *Lyve1* in rat SECs. This is in contrast to expression
341 reported for SC in mice, where *Lyve1* expression is only associated with resident macrophages and not
342 SECs.[12] *Lyve1* expression is controlled by specific signaling pathways, such as those involving *Prox1*,
343 and encodes a hyaluronan receptor that primarily helps regulate the transport of immune cells and fluid
344 through lymphatic vessels.[103] This function is distinct from that of blood vessels, which largely manage
345 nutrient movement and gas exchange; consequently *Lyve1* is not expressed by BECs. However, SC is
346 known to show hybrid characteristics of lymphatic and blood vasculature, expressing BEC-like *Cd34*,

347 *Flt1*, *Nos3*, and LEC-like *Prox1*. Like lymphatic vessels, SC is highly involved in fluid homeostasis and
348 immune cell trafficking from the eye, for which *Lyve1* may play a role. Our data is consistent with this
349 function for *Lyve1* in the SC of rats with expression that is negligible in early SECs but upregulated as
350 the cells mature and acquire a lymphatic-like state.

351 The identification of novel single gene causes of congenital glaucoma has not been forthcoming despite
352 large-scale sequencing efforts. It is likely that there are many undiscovered genes in which strong-effect
353 variants account for a limited proportion of the disease, but these are difficult to identify in individuals
354 or small-sized patient cohorts. Utilizing the transcriptomic resource presented here, interrogation of
355 variants in developing AHOP-expressed genes can now be prioritized. Importantly, 395 genes were
356 detected as selectively upregulated during the development of the TM/SC. Noteworthy genes
357 significantly upregulated by SC-related cells were *Agt*, *Ccl2*, *Cdkl1*, *Chst3*, *Clic2*, *Dapk2*, *Lbp*, *Mmrn1*,
358 *Myzap*, *Tbx1*, and *Trim16*. For TM-related cell types, prominent genes included *Adamtsl3*, *Epha3*,
359 *Fmod*, *Itga11*, *Nkd2*, *Phactr4*, and *Prelp*. These genes are likely critical for the development and/or
360 function of the AHOP and warrant further investigation. We propose prioritization of these genes during
361 patient genome analyses as they represent strong novel candidates for congenital glaucoma-causing
362 variants.

363 It is probable that a proportion of the unresolved disease may not follow single gene/Mendelian
364 inheritance but instead involve complex polygenic mechanisms. Hundreds of genes have already been
365 associated with glaucoma endophenotypes by GWAS, and investigators are now utilizing this
366 knowledge to generate polygenic risk scores (PRS) – an approach that estimates an individual's disease
367 risk based on their overall genetic makeup. This transcriptomic dataset will help adjust the weighting of
368 variants in genes more highly expressed during AHOP tissue development, which in turn will enable the
369 generation of PRS estimates tailored towards early-onset forms of glaucoma.

Materials and methods

Ocular tissue acquisition

All animal procedures performed in the study were in accordance with the ARVO Statement for Use of Animals in Ophthalmic Vision and Research. The ethical principles established by the National Institutes of Health Guide for the Care and Use of Laboratory Animals (revised 2011) were followed. The research protocol was ethically reviewed and approved by the University of Wisconsin–Madison School of Medicine and Public Health Institutional Animal Care and Use Committee.

Fischer 344 (F344/NCrl, Charles River Laboratories) rats, an albino, inbred strain of the common rat (*Rattus norvegicus*), were bred using standard husbandry practices. Staggered breeding pairs were established to collect all 18 limbal tissue strips within a three-day window. To minimize acquisition bias, dissections were performed in six groups, systematically changing the ascertainment order across genders and developmental age (S2 Table). Eyes were removed and immediately placed in ice-cold Hanks' Balanced Salt Solution (HBSS) without calcium. Extraocular muscle was removed, and a scalpel was used to make an incision in the sclera just posterior to the limbus. Fine spring scissors were used to cut circumferentially around the globe to isolate the anterior cup. The lens and retina were removed, and the anterior cup was bisected through the pupil with a scalpel. The iris was trimmed to retain only a small region adjacent to the ciliary body. The opaque sclera was dissected away just posterior to the ciliary body, and the clear cornea was excised immediately anterior to the limbus. The resulting limbal tissue strips were maintained in ice-cold calcium-free HBSS until all three samples in the group were ready for simultaneous dissociation.

Limbal tissue strips were enzymatically dissociated into single cells using a two-step protocol. First, the tissue was digested with Collagenase Type 1 (CLSS-1, 10 mg/mL; Worthington) in HBSS supplemented

392 with calcium and magnesium at 37°C for 1.5 hours, with gentle inversion every 15 minutes. Following
393 centrifugation at 300 RCF for 5 minutes (a condition used for all subsequent centrifugation steps), the
394 pellet was further digested with TrypLE at 37°C for 20 minutes. During this step, samples were inverted
395 at 5 and 10 minutes and gently pipetted with a wide-bore P1000 tip at 15 and 20 minutes to enhance
396 dissociation.

397 After centrifugation, the largely dissociated cells were resuspended in ice-cold DMEM supplemented
398 with 10% FBS. Residual tissue was gently dissociated by pipetting with a regular-bore P1000 tip. The
399 cell suspension was filtered through a 70 µm Flowmi tip, centrifuged, and resuspended in 100 µL by
400 pipetting with a wide-bore P200 tip, followed by a regular-bore P200 tip. The sample was then passed
401 through a 40 µm Flowmi tip. Cell count and viability were assessed with a LUNA FX7, ensuring 11,200
402 viable single cells (>75% viability) were prepared for each sample. Cells were loaded into a well of a
403 Chromium Next GEM Chip G, and Single-Cell 3′ Gene Expression libraries generated following the
404 manufacturer's protocol (Chromium Next GEM Single-Cell 3′ Reagent Kit v3.1 User Guide, Rev D).

405 Single-cell RNA sequencing and bioinformatic processing

406 Eighteen dissociated tissue samples were independently processed through 18 GEM wells for 3' cDNA
407 library construction. A preliminary low-read-deep sequencing run was conducted on an Illumina MiSeq
408 to estimate the total cell counts and reads per cell across libraries. Quality control was performed using
409 UMI-tools.[104] The 18 libraries were balanced, pooled, and deeply sequenced on a single S4 flow cell
410 using the Illumina NovaSeq platform. Demultiplexing was performed with Cell Ranger's mkfastq
411 command, utilizing Illumina's bcl2fastq wrapper. Subsequent alignment, filtering, and UMI counting for
412 each sample was completed using the count command, in accordance with 10x Genomics'
413 documentation. Reads were aligned to the latest rat genome reference (GRCr8, GenBank

414 GCA_036323735.1, Jan 31, 2024) with the mitochondrial reference contig added from an earlier
415 genome build (Rnor_6.0). Alignments included introns to enhance expression sensitivity and excluded
416 pseudogenes to improve mapping quality.

417 Cell Ranger generated barcode matrices for each sample, which were aggregated using the aggr
418 command. Unique GEM well suffixes were appended to barcodes to retain sample identity. Aggregation
419 included depth normalization, ensuring equal average read depth per cell across samples to avoid
420 sequencing depth-related artifacts. As all libraries were sequenced together in a single flow cell, no
421 batch correction was necessary. The final aggregated matrix comprised raw normalized expression data
422 from 126,787 gel bead droplets that were suitable for comparative analyses.

423 Bioinformatic analyses

424 Data analysis was conducted primarily with the Seurat v 5.0.1 R package.[105] A Seurat object was created
425 from the aggregated barcode matrix, including genes expressed in at least five cells. Low-quality cells
426 were filtered out based on the following criteria: UMI count < 3000, fewer than 1200 genes expressed,
427 or mitochondrial gene content > 10%. Mitochondrial content was calculated across 13 protein-coding
428 mitochondrial genes (Mt-co1, Mt-nd6, Mt-atp6, Mt-co2, Mt-co3, Mt-nd3, Mt-nd1, Mt-nd4, Mt-nd5, Mt-
429 atp8, Mt-nd2, Mt-nd4l, Mt-cyb). This filtering reduced the initial 126,787 cells to 90,274 high-quality
430 cells.

431 Multiplets were detected and removed (~4%) using scDblFinder, yielding a final dataset of 86,653 single
432 cells and 29,626 genes. Expression data were normalized using Seurat's NormalizeData function, which
433 scales gene counts per cell to 10,000, followed by log transformation.

434 For dimensional reduction and clustering, Seurat's SCTransform function was used to normalize, scale,
435 and identify variable genes. Principal component analysis was performed using RunPCA, and an elbow

436 plot determined that the first 18 principal components captured most variance. A Shared Nearest
437 Neighbor (SNN) graph was constructed with FindNeighbors, and clustering was done using
438 FindClusters (resolution = 0.1). A two-dimensional Uniform Manifold Approximation and Projection
439 (UMAP) was generated with RunUMAP, visualizing 13 distinct cell-type clusters according to each
440 cell's overall gene expression similarity.

441 Differential gene expression was assessed using the FindMarkers command in conjunction with the
442 Model-based Analysis of Single-cell Transcriptomics (MAST) algorithm - a statistical tool that models
443 gene expression via a zero-inflated hurdle model to account for sparsity specifically in single-cell
444 datasets.[106] For TMCs, the criteria for selective expression were a greater than two log2 fold change
445 upregulation in more than 20% of cells within the TMC subcluster versus all other limbal cells and
446 robust expression (significant UMI counts or highly cluster-specific UMIs at low level). For SECs, as all
447 the VECs are very different to other limbal cells, a more stringent criteria needed to be implemented
448 with expression thresholds set at a greater than two log2 fold change upregulation in more than 30% of
449 cells within the SEC subcluster versus all other limbal cells, less than 10% expression in other limbal
450 cells, and robust expression (significant UMI counts or highly cluster-specific UMIs at low level).

451 UMAP and HeatMap plots were generated using the standard Seurat package commands DimPlot and
452 DoHeatMap, respectively. Customized DotPlot and FeaturePlot (individual gene expression overlayed
453 on UMAP) images were generated using the DotPlot_scCustom and FeaturePlot_scCustom commands
454 within the scCustomize package (https://doi.org/10.5281/zenodo.5706430).[107]

455 Whole mount fluorescent immunohistochemistry

456 Fischer rats were euthanized via decapitation at P4 and P7 or CO2 gas inhalation at P14 and P28. Eyes
457 were rapidly enucleated and placed in ice-cold 1x phosphate buffered saline pH 7.4 (PBS). Eyes were

458 punctured with a 30G needle posterior to limbus, and immersion fixed in 4% paraformaldehyde (PFA) in
459 PBS for 10 minutes at 4°C. Following fixation, tissues were washed in 70% ice-cold molecular biology
460 grade ethanol (EtOH) and stored in fresh 70% EtOH at 4°C. For staining, eyes were transferred to a
461 Kimwipe soaked in ice-cold PBS for dissection. Using spring scissors and fine tip forceps, extraneous
462 tissues such as the conjunctiva, muscle, and tendon were removed, eyes bisected, and lenses extracted.
463 Anterior eye cups were transferred into a dish containing ice-cold PBS where the retina and ciliary body
464 were removed. The tissues were placed into blocking/staining buffer (5% normal donkey serum (Cat.
465 017-000-121, Jackson ImmunoResearch Labs) 0.5% triton x-100, and 0.01% sodium azide in PBS) on a
466 nutator overnight at 4°C. Blocking buffer was replaced with primary antibodies diluted in staining buffer
467 and incubated on a nutator at 4°C for approximately 24 hours. Mouse anti-CD31/PECAM1 (Cat. MA1-
468 80069, Invitrogen) was diluted 1:100, rabbit anti-LYVE-1 (Cat. 67538, Cell Signaling) at 1:500, and
469 goat anti-AIF-1 (Cat. NB100-1028, Novus) at 1:100. Primary antibodies were removed, and eye cups
470 washed three times in PBS containing 0.01% Tween 20 for one hour at room temperature (RT).
471 Secondary antibodies diluted in staining buffer were added and tissues incubated on a nutator at 4°C for
472 approximately 24 hours. Donkey anti-mouse Alexa 405 (Cat. A48257, Invitrogen) was diluted at 1:500,
473 donkey anti-rabbit Alexa 546 (Cat. A10040, Invitrogen) at 1:500, and donkey anti-goat Alexa 647 (Cat.
474 705-605-147, Jackson ImmunoResearch Labs) at 1:500. Following secondary antibody removal, tissues
475 were washed four times with PBS containing 0.01% Tween 20 for 1 hour at RT. Eye cups were
476 transferred into cold PBS and a series of relief cuts were made towards the center that resulted in a
477 flower petal appearance. Tissues were placed on glass microscope slides with the cornea side down,
478 excess fluid removed, and mounted (Shandon-Mount, Cat. 1900331, Epredia) with #1.5 coverslips.
479 Slides were dried for >16 hours at 4°C and imaged with a Nikon A1R confocal microscope using a 20x

480 objective and 23 um pinhole (1 Aery unit). A 75 um Z-stack of 1 um slices was collected, which
481 encompassed all of SC.

482 *In situ* hybridization (RNAscope)

483 Rats were euthanized by decapitation (P7) or CO2 gas inhalation (P14 and P31). The eyes were rapidly
484 enucleated and transferred into ice-cold 4% PFA in 1x PBS, pH 7.4 (4% PFA). Using a scalpel, a large
485 incision was made posteriorly to the limbus to allow rapid PFA access to internal eye structures. Tissues
486 were placed into fresh ice-cold 4% PFA at 4°C for 2 hours. Eyes were dissected in 4% PFA on ice,
487 removing extraneous muscle and tendon, bisecting posterior to the limbus, and removing the lens.
488 Fixation of the anterior eye cups continued in 4% PFA at 4°C for a total of 20 hours. Tissues were
489 processed through an alcohol series, xylene, and embedded in paraffin. Blocks were stored at 4°C in a
490 sealed container with desiccant. Paraffin blocks were sectioned at 5 µm thickness and allowed to dry
491 overnight at RT. Sections were processed for RNAscope following the manufacturers protocol (User
492 Manual for RNAscope Multiplex Fluorescent Reagent Kit v2, UM 323100/rev B/Effective Date:
493 10/11/2022). Mild conditions were used for antigen retrieval (10 minutes) and standard conditions for
494 the protease treatment (30 minutes). Hybridization was performed in a HybEZ II oven (Cat.
495 321710/321720). Details of RNAscope probes are provided in S3 Table, which were used in conjunction
496 with the following Opal dye fluorophores (Akoya Biosciences): Opal 520 (Cat. FP1487001KT), Opal
497 570 (Cat. FP1488001KT), Opal 620 (Cat. FP1495001KT), and Opal 650 (Cat. FP1496001KT). Images
498 were collected with a Nuance Multispectral Imaging System including an Olympus BX43 microscope
499 with 40x objective and Perkin Elmer Nuance software v.3.0.2).

500

501 # Data availability

502 The raw data files from this study have been deposited in the Sequence Read Archive of the National
503 Center for Biotechnology Information (accession no. PRJNA1311507).

504 # Acknowledgments

505 This study was funded by the National Eye Institute (NEI) R21 EY034251 (to ST), and supported by the
506 Margaret Emma Williams Trust Fund to the University of Wisconsin-Madison Department of
507 Ophthalmology and Visual Sciences, an Unrestricted Grant from Research to Prevent Blindness, Inc. to
508 the University of Wisconsin-Madison Department of Ophthalmology and Visual Sciences, and a Core
509 Grant for Vision Research from the National Institutes for Health (NIH) to the University of Wisconsin-
510 Madison (P30 EY016665).

511 The authors utilized the University of Wisconsin-Madison Biotechnology Center's Gene Expression
512 Center (Research Resource Identifier – RRID:SCR_017757) for 10X Genomics scRNAseq library
513 preparation, DNA Sequencing Facility (RRID:SCR_017759) for Illumina sequencing, and
514 Bioinformatics Core Facility (Research Resource Identifier – RRID:SCR_017799) for initial processing
515 of raw scRNAseq data. The authors wish to thank the University of Wisconsin Translational Research
516 Initiatives in Pathology (TRIP) Laboratory, supported by the UW Department of Pathology and
517 Laboratory Medicine, UWCCC (P30 CA014520) and the Office of The Director- NIH (S10 OD023526)
518 for its histology and RNAscope services, and for the use of their facilities. Confocal imaging was
519 facilitated by the University of Wisconsin Optical Imaging Core, and we thank Lance A Rodenkirch for
520 microscopy support.

521 We thank the department chair, Dr. Terri L. Young, for provision of technical support staff, laboratory
522 space, and start-up funding to Dr. Tompson. The authors would also like to thank Dr. Abigail Radcliff in

the laboratory of Dr. Jyoti Watters (UW School of Veterinary Medicine), and Miranda Pamperin, Riley Brutto, Devin Larson, and John Michael in the laboratory of Dr. Edwin Chapman (UW Neuroscience) for providing rat tissues for preliminary studies. We also thank Dr. Stephanie L. Nay for critical review of the manuscript.

References

1. García-Antón MT, Salazar JJ, de Hoz R, et al. Goniodysgenesis variability and activity of CYP1B1 genotypes in primary congenital glaucoma. *PLoS One*. 2017;12(4):e0176386. doi:10.1371/journal.pone.0176386
2. Souma T, Tompson SW, Thomson BR, et al. Angiopoietin receptor TEK mutations underlie primary congenital glaucoma with variable expressivity. *J Clin Invest*. Jul 1 2016;126(7):2575–2587. doi:10.1172/jci85830
3. Thomson BR, Souma T, Tompson SW, et al. Angiopoietin-1 is required for Schlemm's canal development in mice and humans. *J Clin Invest*. Dec 1 2017;127(12):4421–4436. doi:10.1172/jci95545
4. Kuehn MH, Lipsett KA, Menotti-Raymond M, et al. A Mutation in LTBP2 Causes Congenital Glaucoma in Domestic Cats (Felis catus). *PLoS One*. 2016;11(5):e0154412. doi:10.1371/journal.pone.0154412
5. van Zyl T, Yan W, McAdams A, et al. Cell atlas of aqueous humor outflow pathways in eyes of humans and four model species provides insight into glaucoma pathogenesis. *Proc Natl Acad Sci U S A*. May 12 2020;117(19):10339–10349. doi:10.1073/pnas.2001250117

544 6. van Zyl T, Yan W, McAdams AM, Monavarfeshani A, Hageman GS, Sanes JR. Cell atlas
545 of the human ocular anterior segment: Tissue-specific and shared cell types. *Proc Natl Acad Sci*
546 *U S A*. Jul 19 2022;119(29):e2200914119. doi:10.1073/pnas.2200914119
547 7. Patel G, Fury W, Yang H, et al. Molecular taxonomy of human ocular outflow tissues
548 defined by single-cell transcriptomics. *Proc Natl Acad Sci U S A*. Jun 9 2020;117(23):12856–
549 12867. doi:10.1073/pnas.2001896117
550 8. Thomson BR, Liu P, Onay T, et al. Cellular crosstalk regulates the aqueous humor
551 outflow pathway and provides new targets for glaucoma therapies. *Nat Commun*. Oct 18
552 2021;12(1):6072. doi:10.1038/s41467-021-26346-0
553 9. Balasubramanian R, Kizhatil K, Li T, et al. Transcriptomic profiling of Schlemm's canal
554 cells reveals a lymphatic-biased identity and three major cell states. *Elife*. Oct 18
555 2024;13doi:10.7554/eLife.96459
556 10. Stamer WD, Clark AF. The many faces of the trabecular meshwork cell. *Exp Eye Res*.
557 May 2017;158:112–123. doi:10.1016/j.exer.2016.07.009
558 11. Fuchshofer R, Welge-Lüssen U, Lütjen-Drecoll E, Birke M. Biochemical and
559 morphological analysis of basement membrane component expression in corneoscleral and
560 cribriform human trabecular meshwork cells. *Invest Ophthalmol Vis Sci*. Mar 2006;47(3):794–
561 801. doi:10.1167/iovs.05-0292
562 12. Kizhatil K, Ryan M, Marchant JK, Henrich S, John SW. Schlemm's canal is a unique
563 vessel with a combination of blood vascular and lymphatic phenotypes that forms by a novel
564 developmental process. *PLoS Biol*. Jul 2014;12(7):e1001912. doi:10.1371/journal.pbio.1001912
565 13. Park DY, Lee J, Park I, et al. Lymphatic regulator PROX1 determines Schlemm's canal
566 integrity and identity. *J Clin Invest*. Sep 2014;124(9):3960–3974. doi:10.1172/jci75392

567 14. Braakman ST, Moore JE, Jr., Ethier CR, Overby DR. Transport across Schlemm's canal
568 endothelium and the blood-aqueous barrier. *Exp Eye Res*. May 2016;146:17–21.
569 doi:10.1016/j.exer.2015.11.026
570 15. Remé C, Urner U, Aeberhard B. The development of the chamber angle in the rat eye.
571 Morphological characteristics of developmental stages. *Graefes Arch Clin Exp Ophthalmol*.
572 1983;220(3):139–153. doi:10.1007/bf02175946
573 16. Aspelund A, Tammela T, Antila S, et al. The Schlemm's canal is a VEGF-C/VEGFR-3-
574 responsive lymphatic-like vessel. *J Clin Invest*. Sep 2014;124(9):3975–3986.
575 doi:10.1172/jci75395
576 17. Lang AJ, Mirski SE, Cummings HJ, Yu Q, Gerlach JH, Cole SP. Structural organization
577 of the human TOP2A and TOP2B genes. *Gene*. Oct 23 1998;221(2):255–266.
578 doi:10.1016/s0378-1119(98)00468-5
579 18. Gerdes J, Lemke H, Baisch H, Wacker HH, Schwab U, Stein H. Cell cycle analysis of a
580 cell proliferation-associated human nuclear antigen defined by the monoclonal antibody Ki-67. *J*
581 *Immunol*. Oct 1984;133(4):1710–1715.
582 19. Chakarov S, Lim HY, Tan L, et al. Two distinct interstitial macrophage populations
583 coexist across tissues in specific subtissular niches. *Science*. Mar 15
584 2019;363(6432)doi:10.1126/science.aau0964
585 20. Köhler C. Allograft inflammatory factor-1/Ionized calcium-binding adapter molecule 1 is
586 specifically expressed by most subpopulations of macrophages and spermatids in testis. *Cell*
587 *Tissue Res*. Nov 2007;330(2):291–302. doi:10.1007/s00441-007-0474-7

588 21. Hsieh M, Huang PJ, Chou PY, et al. Carbonic Anhydrase VIII (CAVIII) Gene Mediated
589 Colorectal Cancer Growth and Angiogenesis through Mediated miRNA 16-5p. *Biomedicines*.
590 Apr 29 2022;10(5)doi:10.3390/biomedicines10051030
591 22. Yukiura H, Kano K, Kise R, Inoue A, Aoki J. LPP3 localizes LPA6 signalling to non-
592 contact sites in endothelial cells. *J Cell Sci*. Nov 1 2015;128(21):3871–3877.
593 doi:10.1242/jcs.172098
594 23. Icking A, Matt S, Opitz N, Wiesenthal A, Müller-Esterl W, Schilling K. NOSTRIN
595 functions as a homotrimeric adaptor protein facilitating internalization of eNOS. *J Cell Sci*. Nov
596 1 2005;118(Pt 21):5059–5069. doi:10.1242/jcs.02620
597 24. Norrmén C, Ivanov KI, Cheng J, et al. FOXC2 controls formation and maturation of
598 lymphatic collecting vessels through cooperation with NFATc1. *J Cell Biol*. May 4
599 2009;185(3):439–457. doi:10.1083/jcb.200901104
600 25. Valdembri D, Regano D, Maione F, Giraudo E, Serini G. Class 3 semaphorins in
601 cardiovascular development. *Cell Adh Migr*. Nov 2016;10(6):641–651.
602 doi:10.1080/19336918.2016.1212805
603 26. Aghajanian H, Choi C, Ho VC, Gupta M, Singh MK, Epstein JA. Semaphorin 3d and
604 semaphorin 3e direct endothelial motility through distinct molecular signaling pathways. *J Biol*
605 *Chem*. Jun 27 2014;289(26):17971–17979. doi:10.1074/jbc.M113.544833
606 27. Lee DJ, Kim P, Kim HY, et al. MAST4 regulates stem cell maintenance with DLX3 for
607 epithelial development and amelogenesis. *Exp Mol Med*. Jul 2024;56(7):1606–1619.
608 doi:10.1038/s12276-024-01264-5
609 28. Matsui J, Wakabayashi T, Asada M, Yoshimatsu K, Okada M. Stem cell factor/c-kit
610 signaling promotes the survival, migration, and capillary tube formation of human umbilical vein

611 endothelial cells. *J Biol Chem*. Apr 30 2004;279(18):18600–18607.
612 doi:10.1074/jbc.M311643200
613 29. Koch AE, Halloran MM, Haskell CJ, Shah MR, Polverini PJ. Angiogenesis mediated by
614 soluble forms of E-selectin and vascular cell adhesion molecule-1. *Nature*. Aug 10
615 1995;376(6540):517–519. doi:10.1038/376517a0
616 30. Buschman MD, Bromann PA, Cejudo-Martin P, Wen F, Pass I, Courtneidge SA. The
617 novel adaptor protein Tks4 (SH3PXD2B) is required for functional podosome formation. *Mol*
618 *Biol Cell*. Mar 2009;20(5):1302–1311. doi:10.1091/mbc.e08-09-0949
619 31. Hubmacher D, Schneider M, Berardinelli SJ, et al. Unusual life cycle and impact on
620 microfibril assembly of ADAMTS17, a secreted metalloprotease mutated in genetic eye disease.
621 *Sci Rep*. Feb 8 2017;7:41871. doi:10.1038/srep41871
622 32. Craige SM, Chen K, Pei Y, et al. NADPH oxidase 4 promotes endothelial angiogenesis
623 through endothelial nitric oxide synthase activation. *Circulation*. Aug 9 2011;124(6):731–740.
624 doi:10.1161/circulationaha.111.030775
625 33. Watanabe K, Hasegawa Y, Yamashita H, et al. Vasohibin as an endothelium-derived
626 negative feedback regulator of angiogenesis. *J Clin Invest*. Oct 2004;114(7):898–907.
627 doi:10.1172/jci21152
628 34. Wick N, Saharinen P, Saharinen J, et al. Transcriptomal comparison of human dermal
629 lymphatic endothelial cells ex vivo and in vitro. *Physiol Genomics*. Jan 17 2007;28(2):179–192.
630 doi:10.1152/physiolgenomics.00037.2006
631 35. Rousseau S, Houle F, Landry J, Huot J. p38 MAP kinase activation by vascular
632 endothelial growth factor mediates actin reorganization and cell migration in human endothelial
633 cells. *Oncogene*. Oct 1997;15(18):2169–2177. doi:10.1038/sj.onc.1201380

634 36. Zhu Q, Kim YH, Wang D, Oh SP, Luo K. SnoN facilitates ALK1-Smad1/5 signaling
635 during embryonic angiogenesis. *J Cell Biol*. Sep 16 2013;202(6):937–950.
636 doi:10.1083/jcb.201208113
637 37. Mannan A, Dhiamn S, Garg N, Singh TG. Pharmacological modulation of Sonic
638 Hedgehog signaling pathways in Angiogenesis: A mechanistic perspective. *Dev Biol*. Dec
639 2023;504:58–74. doi:10.1016/j.ydbio.2023.09.009
640 38. Elbitar S, Renard M, Arnaud P, et al. Pathogenic variants in THSD4, encoding the
641 ADAMTS-like 6 protein, predispose to inherited thoracic aortic aneurysm. *Genet Med*. Jan
642 2021;23(1):111–122. doi:10.1038/s41436-020-00947-4
643 39. Gunn MD, Tangemann K, Tam C, Cyster JG, Rosen SD, Williams LT. A chemokine
644 expressed in lymphoid high endothelial venules promotes the adhesion and chemotaxis of naive
645 T lymphocytes. *Proc Natl Acad Sci U S A*. Jan 6 1998;95(1):258–263. doi:10.1073/pnas.95.1.258
646 40. Vaahtomeri K, Moussion C, Hauschild R, Sixt M. Shape and Function of Interstitial
647 Chemokine CCL21 Gradients Are Independent of Heparan Sulfates Produced by Lymphatic
648 Endothelium. *Front Immunol*. 2021;12:630002. doi:10.3389/fimmu.2021.630002
649 41. Choi D, Park E, Jung E, et al. Laminar flow downregulates Notch activity to promote
650 lymphatic sprouting. *J Clin Invest*. Apr 3 2017;127(4):1225–1240. doi:10.1172/jci87442
651 42. Choi D, Park E, Yu RP, et al. Piezo1-Regulated Mechanotransduction Controls Flow-
652 Activated Lymphatic Expansion. *Circ Res*. Jul 8 2022;131(2):e2–e21.
653 doi:10.1161/circresaha.121.320565
654 43. Zhao Y, Lin S. Essential role of SH3-domain GRB2-like 3 for vascular lumen
655 maintenance in zebrafish. *Arterioscler Thromb Vasc Biol*. Jun 2013;33(6):1280–1286.
656 doi:10.1161/atvbaha.112.301025

657 44. Black JA, Waxman SG. Noncanonical roles of voltage-gated sodium channels. *Neuron*.
658 Oct 16 2013;80(2):280–291. doi:10.1016/j.neuron.2013.09.012
659 45. Wasik A, Ratajczak-Wielgomas K, Badzinski A, Dziegiel P, Podhorska-Okolow M. The
660 Role of Periostin in Angiogenesis and Lymphangiogenesis in Tumors. *Cancers (Basel)*. Aug 30
661 2022;14(17)doi:10.3390/cancers14174225
662 46. De Luca F, Kha M, Swärd K, Johansson ME. Identification of ARMH4 and WIPF3 as
663 human podocyte proteins with potential roles in immunomodulation and cytoskeletal dynamics.
664 *PLoS One*. 2023;18(1):e0280270. doi:10.1371/journal.pone.0280270
665 47. Vreeken D, Bruikman CS, Stam W, et al. Downregulation of Endothelial Plexin A4
666 Under Inflammatory Conditions Impairs Vascular Integrity. *Front Cardiovasc Med*.
667 2021;8:633609. doi:10.3389/fcvm.2021.633609
668 48. Morishita T, Tsutsui M, Shimokawa H, et al. Vasculoprotective roles of neuronal nitric
669 oxide synthase. *Faseb j*. Dec 2002;16(14):1994–1996. doi:10.1096/fj.02-0155fje
670 49. Kuek V, Yang Z, Chim SM, et al. NPNT is Expressed by Osteoblasts and Mediates
671 Angiogenesis via the Activation of Extracellular Signal-regulated Kinase. *Sci Rep*. Oct 26
672 2016;6:36210. doi:10.1038/srep36210
673 50. Simonson B, Chaffin M, Hill MC, et al. Single-nucleus RNA sequencing in ischemic
674 cardiomyopathy reveals common transcriptional profile underlying end-stage heart failure. *Cell*
675 *Rep*. Feb 28 2023;42(2):112086. doi:10.1016/j.celrep.2023.112086
676 51. Arystarkhova E. Beneficial Renal and Pancreatic Phenotypes in a Mouse Deficient in
677 FXYD2 Regulatory Subunit of Na,K-ATPase. *Front Physiol*. 2016;7:88.
678 doi:10.3389/fphys.2016.00088

679 52. Williams AL, Bohnsack BL. The Ocular Neural Crest: Specification, Migration, and Then
680 What? *Front Cell Dev Biol*. 2020;8:595896. doi:10.3389/fcell.2020.595896
681 53. Cvekl A, Tamm ER. Anterior eye development and ocular mesenchyme: new insights
682 from mouse models and human diseases. *Bioessays*. Apr 2004;26(4):374–386.
683 doi:10.1002/bies.20009
684 54. Gong HY, Trinkaus-Randall V, Freddo TF. Ultrastructural immunocytochemical
685 localization of elastin in normal human trabecular meshwork. *Curr Eye Res*. Oct
686 1989;8(10):1071–1082. doi:10.3109/02713688908997400
687 55. Xue W, Wallin R, Olmsted-Davis EA, Borrás T. Matrix GLA protein function in human
688 trabecular meshwork cells: inhibition of BMP2-induced calcification process. *Invest Ophthalmol*
689 *Vis Sci*. Mar 2006;47(3):997–1007. doi:10.1167/iovs.05-1106
690 56. Chowdhury UR, Jea SY, Oh DJ, Rhee DJ, Fautsch MP. Expression profile of the
691 matricellular protein osteopontin in primary open-angle glaucoma and the normal human eye.
692 *Invest Ophthalmol Vis Sci*. Aug 16 2011;52(9):6443–6451. doi:10.1167/iovs.11-7409
693 57. Young TL, Whisenhunt KN, Jin J, et al. SVEP1 as a Genetic Modifier of TEK-Related
694 Primary Congenital Glaucoma. *Invest Ophthalmol Vis Sci*. Oct 1 2020;61(12):6.
695 doi:10.1167/iovs.61.12.6
696 58. Narooie-Nejad M, Paylakhi SH, Shojaee S, et al. Loss of function mutations in the gene
697 encoding latent transforming growth factor beta binding protein 2, LTBP2, cause primary
698 congenital glaucoma. *Hum Mol Genet*. Oct 15 2009;18(20):3969–3977.
699 doi:10.1093/hmg/ddp338
700 59. Lütjen-Drecoll E. Functional morphology of the trabecular meshwork in primate eyes.
701 *Prog Retin Eye Res*. Jan 1999;18(1):91–119. doi:10.1016/s1350-9462(98)00011-1

702 60. Shuman MA, Polansky JR, Merkel C, Alvarado JA. Tissue plasminogen activator in
703 cultured human trabecular meshwork cells. Predominance of enzyme over plasminogen activator
704 inhibitor. *Invest Ophthalmol Vis Sci*. Mar 1988;29(3):401–405.
705 61. De La Paz MA, Epstein DL. Effect of age on superoxide dismutase activity of human
706 trabecular meshwork. *Invest Ophthalmol Vis Sci*. Aug 1996;37(9):1849–1853.
707 62. Liton PB, Luna C, Bodman M, Hong A, Epstein DL, Gonzalez P. Induction of IL-6
708 expression by mechanical stress in the trabecular meshwork. *Biochem Biophys Res Commun*.
709 Dec 2 2005;337(4):1229–1236. doi:10.1016/j.bbrc.2005.09.182
710 63. Rittig M, Flügel C, Prehm P, Lütjen-Drecoll E. Hyaluronan synthase immunoreactivity in
711 the anterior segment of the primate eye. *Graefes Arch Clin Exp Ophthalmol*. Jun
712 1993;231(6):313–317. doi:10.1007/bf00919026
713 64. Usui T, Nakajima F, Ideta R, et al. Hyaluronan synthase in trabecular meshwork cells. *Br*
714 *J Ophthalmol*. Mar 2003;87(3):357–360. doi:10.1136/bjo.87.3.357
715 65. Keller KE, Vranka JA, Haddadin RI, et al. The effects of tenascin C knockdown on
716 trabecular meshwork outflow resistance. *Invest Ophthalmol Vis Sci*. Aug 19 2013;54(8):5613–
717 5623. doi:10.1167/iovs.13-11620
718 66. Flügel-Koch C, Ohlmann A, Fuchshofer R, Welge-Lüssen U, Tamm ER.
719 Thrombospondin-1 in the trabecular meshwork: localization in normal and glaucomatous eyes,
720 and induction by TGF-beta1 and dexamethasone in vitro. *Exp Eye Res*. Nov 2004;79(5):649–
721 663. doi:10.1016/j.exer.2004.07.005
722 67. Siegner A, May CA, Welge-Lüssen UW, Bloemendal H, Lütjen-Drecoll E. alpha B-
723 crystallin in the primate ciliary muscle and trabecular meshwork. *Eur J Cell Biol*. Oct
724 1996;71(2):165–169.

725 68. Walsh JG, Cullen SP, Sheridan C, Lüthi AU, Gerner C, Martin SJ. Executioner caspase-3
726 and caspase-7 are functionally distinct proteases. *Proc Natl Acad Sci U S A*. Sep 2
727 2008;105(35):12815–12819. doi:10.1073/pnas.0707715105
728 69. Matsumoto K, Shionyu M, Go M, et al. Distinct interaction of versican/PG-M with
729 hyaluronan and link protein. *J Biol Chem*. Oct 17 2003;278(42):41205–41212.
730 doi:10.1074/jbc.M305060200
731 70. Keller KE, Bradley JM, Vranka JA, Acott TS. Segmental versican expression in the
732 trabecular meshwork and involvement in outflow facility. *Invest Ophthalmol Vis Sci*. Jul 7
733 2011;52(8):5049–5057. doi:10.1167/iovs.10-6948
734 71. McCulloch DR, Nelson CM, Dixon LJ, et al. ADAMTS metalloproteases generate active
735 versican fragments that regulate interdigital web regression. *Dev Cell*. Nov 2009;17(5):687–698.
736 doi:10.1016/j.devcel.2009.09.008
737 72. Dua HS, Faraj LA, Branch MJ, et al. The collagen matrix of the human trabecular
738 meshwork is an extension of the novel pre-Descemet's layer (Dua's layer). *Br J Ophthalmol*. May
739 2014;98(5):691–697. doi:10.1136/bjophthalmol-2013-304593
740 73. Fang J, Hou F, Wu S, et al. Piezo2 downregulation via the Cre-lox system affects aqueous
741 humor dynamics in mice. *Mol Vis*. 2021;27:354–364.
742 74. Docheva D, Hunziker EB, Fassler R, Brandau O. Tenomodulin is necessary for tenocyte
743 proliferation and tendon maturation. *Mol Cell Biol*. Jan 2005;25(2):699–705.
744 doi:10.1128/MCB.25.2.699-705.2005
745 75. Runager K, Enghild JJ, Klintworth GK. Focus on molecules: Transforming growth factor
746 beta induced protein (TGFBIp). *Exp Eye Res*. Oct 2008;87(4):298–299.
747 doi:10.1016/j.exer.2007.12.001

748 76. Harada K, Yamazaki T, Iwata C, et al. Identification of targets of Prox1 during in vitro
749 vascular differentiation from embryonic stem cells: functional roles of HoxD8 in
750 lymphangiogenesis. *J Cell Sci*. Nov 1 2009;122(Pt 21):3923–3930. doi:10.1242/jcs.052324
751 77. Ma AS, Grigg JR, Jamieson RV. Phenotype-genotype correlations and emerging
752 pathways in ocular anterior segment dysgenesis. *Hum Genet*. Sep 2019;138(8-9):899–915.
753 doi:10.1007/s00439-018-1935-7
754 78. Siggs OM, Souzeau E, Pasutto F, et al. Prevalence of FOXC1 Variants in Individuals
755 With a Suspected Diagnosis of Primary Congenital Glaucoma. *JAMA Ophthalmol*. Apr 1
756 2019;137(4):348–355. doi:10.1001/jamaophthalmol.2018.5646
757 79. Siggs OM, Souzeau E, Taranath DA, et al. Biallelic CPAMD8 Variants Are a Frequent
758 Cause of Childhood and Juvenile Open-Angle Glaucoma. *Ophthalmology*. Jun 2020;127(6):758–
759 766. doi:10.1016/j.ophtha.2019.12.024
760 80. Tham YC, Li X, Wong TY, Quigley HA, Aung T, Cheng CY. Global prevalence of
761 glaucoma and projections of glaucoma burden through 2040: a systematic review and meta-
762 analysis. *Ophthalmology*. Nov 2014;121(11):2081–2090. doi:10.1016/j.ophtha.2014.05.013
763 81. Kwon YH, Fingert JH, Kuehn MH, Alward WL. Primary open-angle glaucoma. *N Engl J*
764 *Med*. Mar 12 2009;360(11):1113–1124. doi:10.1056/NEJMra0804630
765 82. Gharahkhani P, Jorgenson E, Hysi P, et al. Genome-wide meta-analysis identifies 127
766 open-angle glaucoma loci with consistent effect across ancestries. *Nat Commun*. Feb 24
767 2021;12(1):1258. doi:10.1038/s41467-020-20851-4
768 83. Han X, Gharahkhani P, Hamel AR, et al. Large-scale multitrait genome-wide association
769 analyses identify hundreds of glaucoma risk loci. *Nat Genet*. Jul 2023;55(7):1116–1125.
770 doi:10.1038/s41588-023-01428-5

771 84. Zhao Y, Wang S, Sorenson CM, et al. Cyp1b1 mediates periostin regulation of trabecular
772 meshwork development by suppression of oxidative stress. *Mol Cell Biol*. Nov
773 2013;33(21):4225–4240. doi:10.1128/mcb.00856-13
774 85. Yarishkin O, Phuong TTT, Baumann JM, et al. Piezo1 channels mediate trabecular
775 meshwork mechanotransduction and promote aqueous fluid outflow. *J Physiol*. Jan
776 2021;599(2):571–592. doi:10.1113/JP281011
777 86. Du J, Thomson BR, Onay T, Quaggin SE. Endothelial Tyrosine Kinase Tie1 Is Required
778 for Normal Schlemm's Canal Development-Brief Report. *Arterioscler Thromb Vasc Biol*. Mar
779 2022;42(3):348–351. doi:10.1161/ATVBAHA.121.316692
780 87. Cheong SS, Hentschel L, Davidson AE, et al. Mutations in CPAMD8 Cause a Unique
781 Form of Autosomal-Recessive Anterior Segment Dysgenesis. *Am J Hum Genet*. Dec 1
782 2016;99(6):1338–1352. doi:10.1016/j.ajhg.2016.09.022
783 88. Dulle JE, Rübsam A, Garnai SJ, Pawar HS, Fort PE. BetaB2-crystallin mutations
784 associated with cataract and glaucoma leads to mitochondrial alterations in lens epithelial cells
785 and retinal neurons. *Exp Eye Res*. Feb 2017;155:85–90. doi:10.1016/j.exer.2017.01.005
786 89. Garnai SJ, Huyghe JR, Reed DM, et al. Congenital cataracts: de novo gene conversion
787 event in CRYBB2. *Mol Vis*. 2014;20:1579–1593.
788 90. Liu H, Bell K, Herrmann A, et al. Crystallins Play a Crucial Role in Glaucoma and
789 Promote Neuronal Cell Survival in an In Vitro Model Through Modulating Müller Cell
790 Secretion. *Invest Ophthalmol Vis Sci*. Jul 8 2022;63(8):3. doi:10.1167/iovs.63.8.3
791 91. Semina EV, Brownell I, Mintz-Hittner HA, Murray JC, Jamrich M. Mutations in the
792 human forkhead transcription factor FOXE3 associated with anterior segment ocular dysgenesis
793 and cataracts. *Hum Mol Genet*. Feb 1 2001;10(3):231–236. doi:10.1093/hmg/10.3.231

794 92. Blixt A, Mahlapuu M, Aitola M, Pelto-Huikko M, Enerbäck S, Carlsson P. A forkhead
795 gene, FoxE3, is essential for lens epithelial proliferation and closure of the lens vesicle. *Genes*
796 *Dev*. Jan 15 2000;14(2):245–254.
797 93. Semina EV, Ferrell RE, Mintz-Hittner HA, et al. A novel homeobox gene PITX3 is
798 mutated in families with autosomal-dominant cataracts and ASMD. *Nat Genet*. Jun
799 1998;19(2):167–170. doi:10.1038/527
800 94. Nair KS, Hmani-Aifa M, Ali Z, et al. Alteration of the serine protease PRSS56 causes
801 angle-closure glaucoma in mice and posterior microphthalmia in humans and mice. *Nat Genet*.
802 Jun 2011;43(6):579–584. doi:10.1038/ng.813
803 95. Rad A, Altunoglu U, Miller R, et al. MAB21L1 loss of function causes a syndromic
804 neurodevelopmental disorder with distinctive cerebellar, ocular, craniofacial and genital features
805 (COFG syndrome). *J Med Genet*. May 2019;56(5):332–339. doi:10.1136/jmedgenet-2018-
806 105623
807 96. Deml B, Kariminejad A, Borujerdi RH, Muheisen S, Reis LM, Semina EV. Mutations in
808 MAB21L2 result in ocular Coloboma, microcornea and cataracts. *PLoS Genet*.
809 2015;11(2):e1005002. doi:10.1371/journal.pgen.1005002
810 97. Bruel AL, Masurel-Paulet A, Rivière JB, et al. Autosomal recessive truncating MAB21L1
811 mutation associated with a syndromic scrotal agenesis. *Clin Genet*. Feb 2017;91(2):333–338.
812 doi:10.1111/cge.12794
813 98. Seese SE, Deml B, Muheisen S, Sorokina E, Semina EV. Genetic disruption of zebrafish
814 mab21l1 reveals a conserved role in eye development and affected pathways. *Dev Dyn*. Aug
815 2021;250(8):1056–1073. doi:10.1002/dvdy.312

816 99. Wawersik S, Maas RL. Vertebrate eye development as modeled in Drosophila. *Hum Mol*
817 *Genet*. Apr 12 2000;9(6):917–925. doi:10.1093/hmg/9.6.917
818 100. Hanson IM. PAX6 and congenital eye malformations. *Pediatr Res*. Dec 2003;54(6):791–
819 796. doi:10.1203/01.Pdr.0000096455.00657.98
820 101. Baulmann DC, Ohlmann A, Flügel-Koch C, Goswami S, Cvekl A, Tamm ER. Pax6
821 heterozygous eyes show defects in chamber angle differentiation that are associated with a wide
822 spectrum of other anterior eye segment abnormalities. *Mech Dev*. Oct 2002;118(1-2):3–17.
823 doi:10.1016/s0925-4773(02)00260-5
824 102. Ferre-Fernández JJ, Aroca-Aguilar JD, Medina-Trillo C, et al. Whole-Exome Sequencing
825 of Congenital Glaucoma Patients Reveals Hypermorphic Variants in GPATCH3, a New Gene
826 Involved in Ocular and Craniofacial Development. *Sci Rep*. Apr 11 2017;7:46175.
827 doi:10.1038/srep46175
828 103. Banerji S, Ni J, Wang SX, et al. LYVE-1, a new homologue of the CD44 glycoprotein, is
829 a lymph-specific receptor for hyaluronan. *J Cell Biol*. Feb 22 1999;144(4):789–801.
830 doi:10.1083/jcb.144.4.789
831 104. Smith T, Heger A, Sudbery I. UMI-tools: modeling sequencing errors in Unique
832 Molecular Identifiers to improve quantification accuracy. *Genome Res*. Mar 2017;27(3):491–
833 499. doi:10.1101/gr.209601.116
834 105. Hao Y, Stuart T, Kowalski MH, et al. Dictionary learning for integrative, multimodal and
835 scalable single-cell analysis. *Nat Biotechnol*. Feb 2024;42(2):293–304. doi:10.1038/s41587-023-
836 01767-y

106. Nguyen HCT, Baik B, Yoon S, Park T, Nam D. Benchmarking integration of single-cell differential expression. *Nat Commun*. Mar 21 2023;14(1):1570. doi:10.1038/s41467-023-37126-3

107. *scCustomize: Custom Visualizations & Functions for Streamlined Analyses of Single Cell Sequencing*. Version 2.1.2. Zenodo; 2024. https://samuel-marsh.github.io/scCustomize/

Figure legends

Fig 1. Route of aqueous humor outflow from the eye.

H&E-stained tissue section from a mature (P80) rat eye showing the location of the AHOP at the junction of the cornea and iris. Aqueous humor exits the eye (blue arrows) through the trabecular meshwork (TM) and Schlemm's canal (SC), which encircle the anterior chamber. Tissues dissected for scRNAseq profiling are highlighted (blue dashed box) and shown relative to a whole eye (insert).

Fig 2. Morphology of dissected developing AHOP tissues and resulting scRNAseq clustering of complete limbal dataset.

(A) H&E-stained anterior eye sections highlighting the AHOP tissues at P8, P15, and P28. Labels show primitive TM (PTM), primitive SC (PSC), trabecular meshwork (TM), Schlemm's canal (SC), and Fontana's spaces (FS). Scale bars 50µm. (B) Clustering of single-cell profiles visualized by two-dimensional Uniform Manifold Approximation and Projection (UMAP). The 13 major clusters are distinguished by different colors and numbered (C0-C12) by descending cell population. Cell type identities assigned by key marker gene expression (Fig S1) are smooth muscle cells (SMC), fibroblasts

858 (FIBR), pigmented epithelium (PIEP), pericytes (PERI), melanocytes (MELA), monocytes-1 (MON1),
859 nonpigmented ciliary epithelium (NPCE), surface epithelium (EPI), vescular endothelial cells (VEC),
860 Schwann cells (SCHW), lymphocytes (LYMP), proliferating mesenchyme (PMES), and monocytes-2
861 (MON2).

862

863 **Fig 3. As SC develops in rats, a population of SECs express *Lyve1* as they take on a more**
864 **lymphatic phenotype.**

865 (A) Reclustering of 3,155 VECs from the limbal C8 population visualized by UMAP in nine subtypes
866 (VEC0-VEC8). (B) *Lyve1* expression throughout the VEC dataset (normalized log2 fold change
867 expression). (C) Whole mount anterior cup tissues stained with Pecam1 (blue) to visualize SC, Aif1+
868 (cyan) macrophages, and Lyve1+ (red) subsets of macrophages and SECs. Macrophage-aided fusion of
869 rudimentary vessels shown at P4 (arrow). Images oriented SC inner wall down. Scale bars 50µm.

870

871 **Fig 4. Cellular subtypes and associated gene expression within the Schlemm's canal endothelial**
872 **cell population during development.**

873 (A) UMAP plot of the six SEC subpopulations at the three developmental timepoints. (B) Dot plot of
874 key marker gene expression distinguishing SEC subtypes. The dot diameter represents the percentage of
875 each cell type expressing the gene, while the color denotes the scaled average expression within the
876 cluster.

877 **Fig 5. Limbal expression of *Myoc*, *Angpt1*, *Svep1*, and *Ltbp2* in TMCs (fibroblast-like cells, C1).**

878 Gene expression derived from scRNAseq data (normalized log2 fold change, left) alongside tissue
879 sections stained by ISH (right) at each age. All ISH images are oriented the same as the first panel with
880 the anterior side (A, closer to the pupil) on the left, posterior side (P, closer to the retina) on the right, the
881 outer side of the eye (O) towards the top, and the inner side (I) towards the bottom. TM location is
882 highlighted between dashed white lines and the position of SC is displayed as a red ellipse.

883

884 **Fig 6. Cellular subtypes and associated gene expression within the developing trabecular**
885 **meshwork cell population.**

886 (A) UMAP plot of seven TMC-like subtypes (TMC0-TMC6) derived from FBL0 at each age. (B) Dot
887 plot of key marker gene expression distinguishing TMC-like subtypes.

888

889 **Fig 7. Dot plot visualization of the relative expression of 395 genes selectively expressed in SC- and**
890 **TM-related cell clusters.**

891 Gene names are listed along the y-axis and cell type cluster names are shown along the x-axis; six SC-
892 related clusters (SEC0-SEC5) and seven TM-related clusters (TMC0-TMC6). Average gene expression
893 is relative to other SC and TM clusters.

894

895 **Fig 8. Dot plot visualization of the relative expression of 44 Mendelian congenital glaucoma-**
896 **associated genes between SEC and TMC subtypes.**

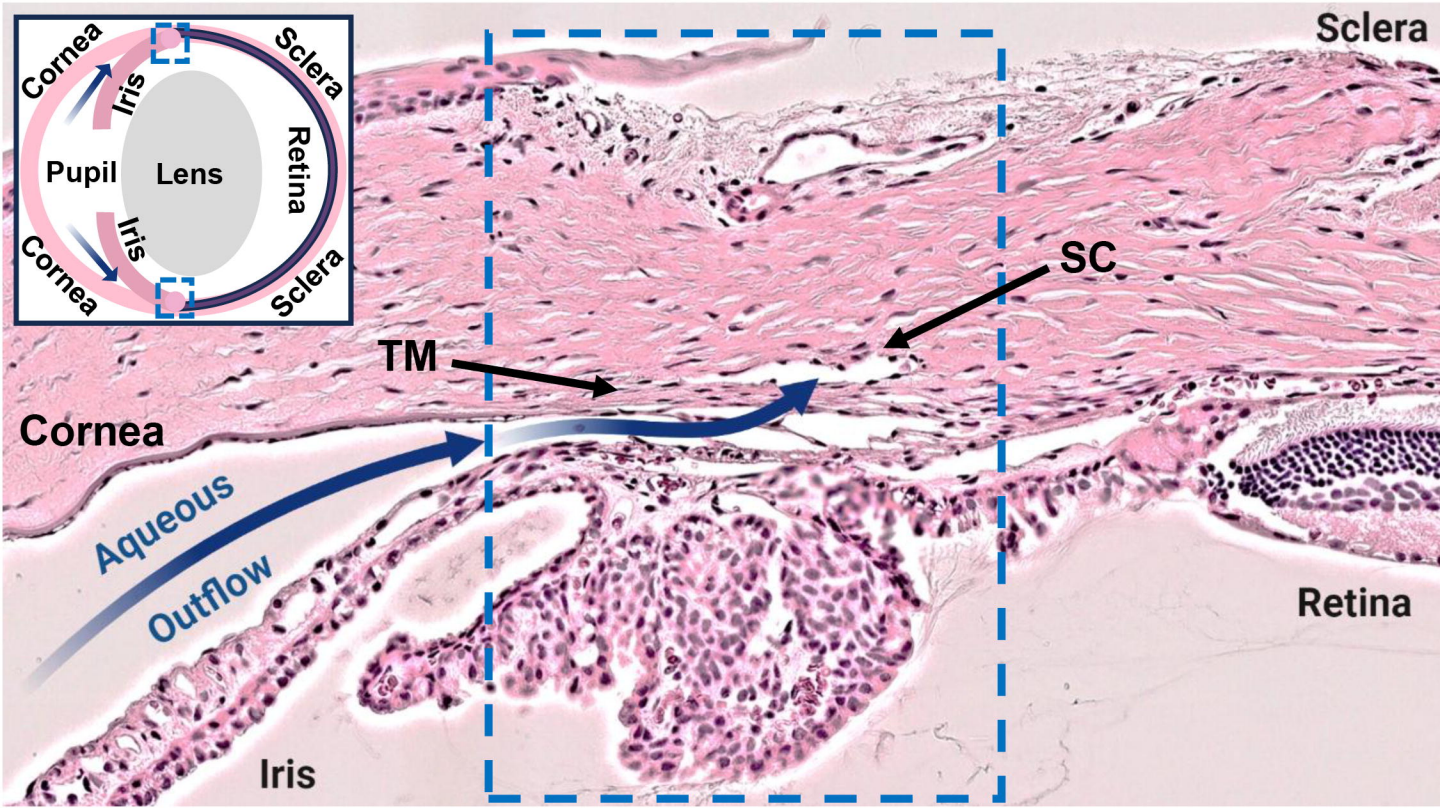
Cornea
Iris
Sclera
Pupil
Lens
Retina
Iris
Cornea
Sclera
Sclera
SC
TM
Cornea
Aqueous
Outflow
Retina
Iris

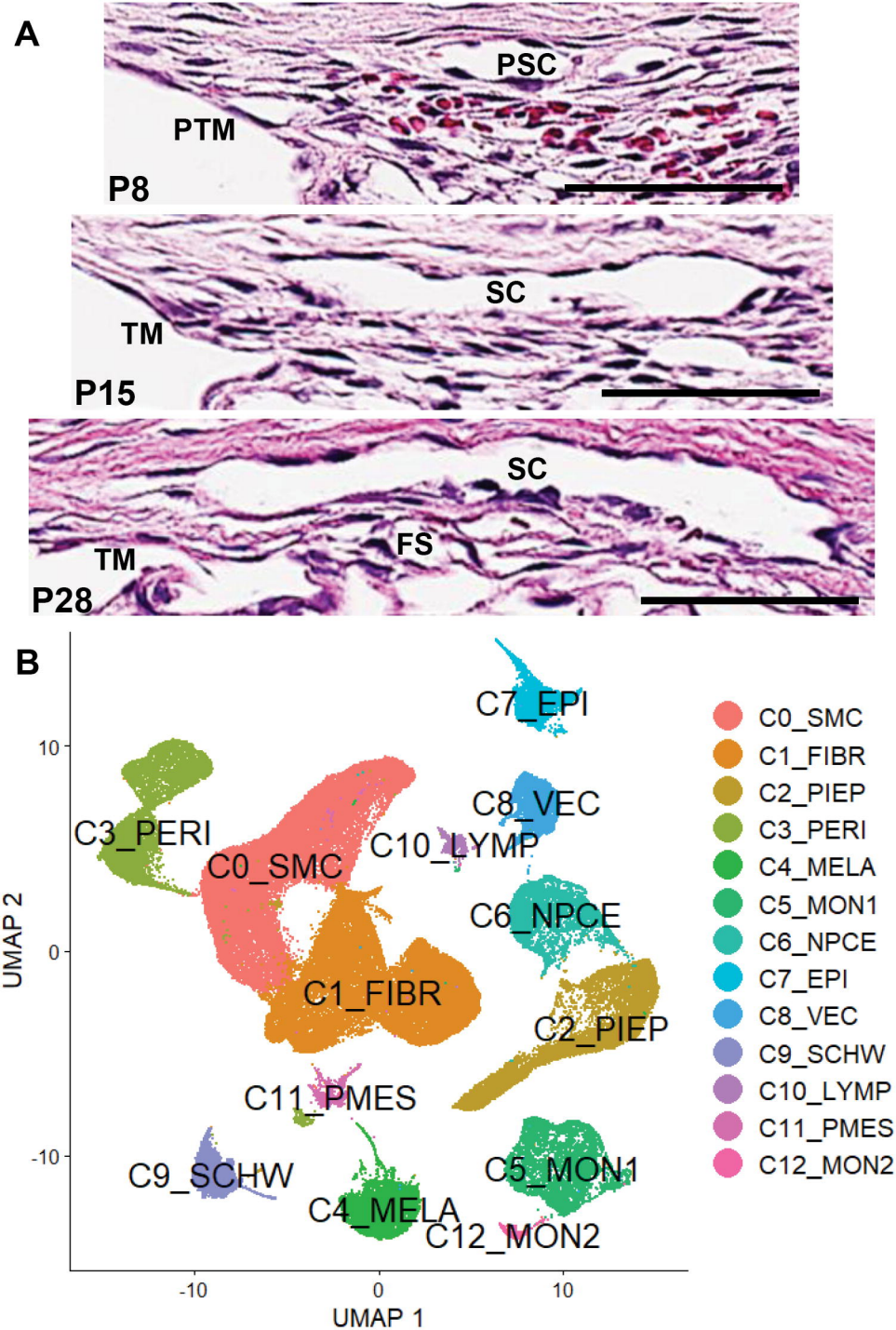
A
PSC
PTM
P8
SC
TM
P15
SC
FS
TM
P28
B
C7_EPI
C8_VEC
C3_PERI
C10_LYMP
C0_SMC
C6_NPCE
C1_FIBR
C2_PIEP
C11_PMES
C9_SCHW
C5_MON1
C4_MELA
C12_MON2
10
0
-10
UMAP 2
-10
0
10
UMAP 1
C0_SMC
C1_FIBR
C2_PIEP
C3_PERI
C4_MELA
C5_MON1
C6_NPCE
C7_EPI
C8_VEC
C9_SCHW
C10_LYMP
C11_PMES
C12_MON2

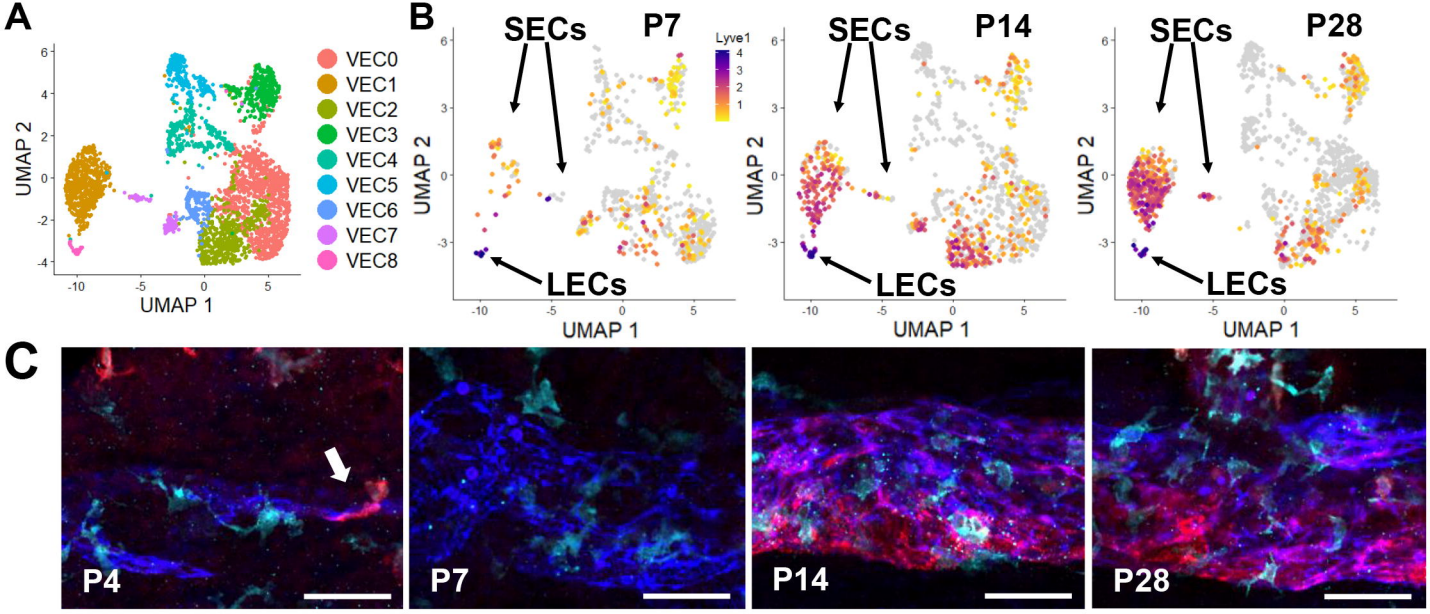
A
UMAP 2
UMAP 1
VEC0
VEC1
VEC2
VEC3
VEC4
VEC5
VEC6
VEC7
VEC8
B
SECs
P7
Lyve1
LECs
SECs
P14
LECs
SECs
P28
LECs
UMAP 2
UMAP 1
C
P4
P7
P14
P28

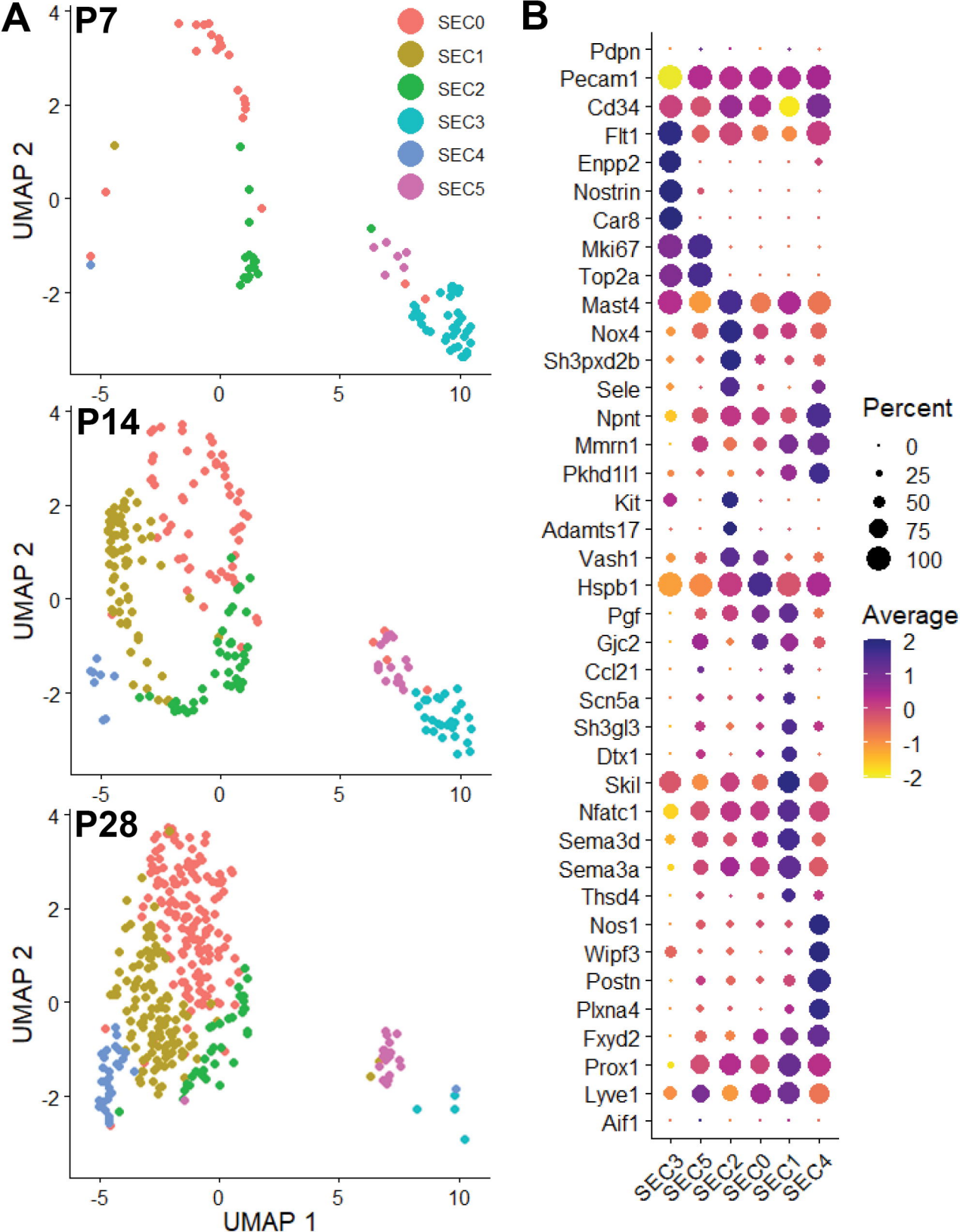
A
P7
P14
P28
SEC0
SEC1
SEC2
SEC3
SEC4
SEC5
UMAP 2
UMAP 1
B
Pdpn
Pecam1
Cd34
Flt1
Enpp2
Nostrin
Car8
Mki67
Top2a
Mast4
Nox4
Sh3pxd2b
Sele
Npnt
Mmrn1
Pkhd1l1
Kit
Adamts17
Vash1
Hspb1
Pgf
Gjc2
Ccl21
Scn5a
Sh3gl3
Dtx1
Skil
Nfatc1
Sema3d
Sema3a
Thsd4
Nos1
Wipf3
Postn
Plxna4
Fxyd2
Prox1
Lyve1
Aif1
SEC3
SEC5
SEC2
SEC0
SEC1
SEC4
Percent
0
25
50
75
100
Average
2
1
0
-1
-2

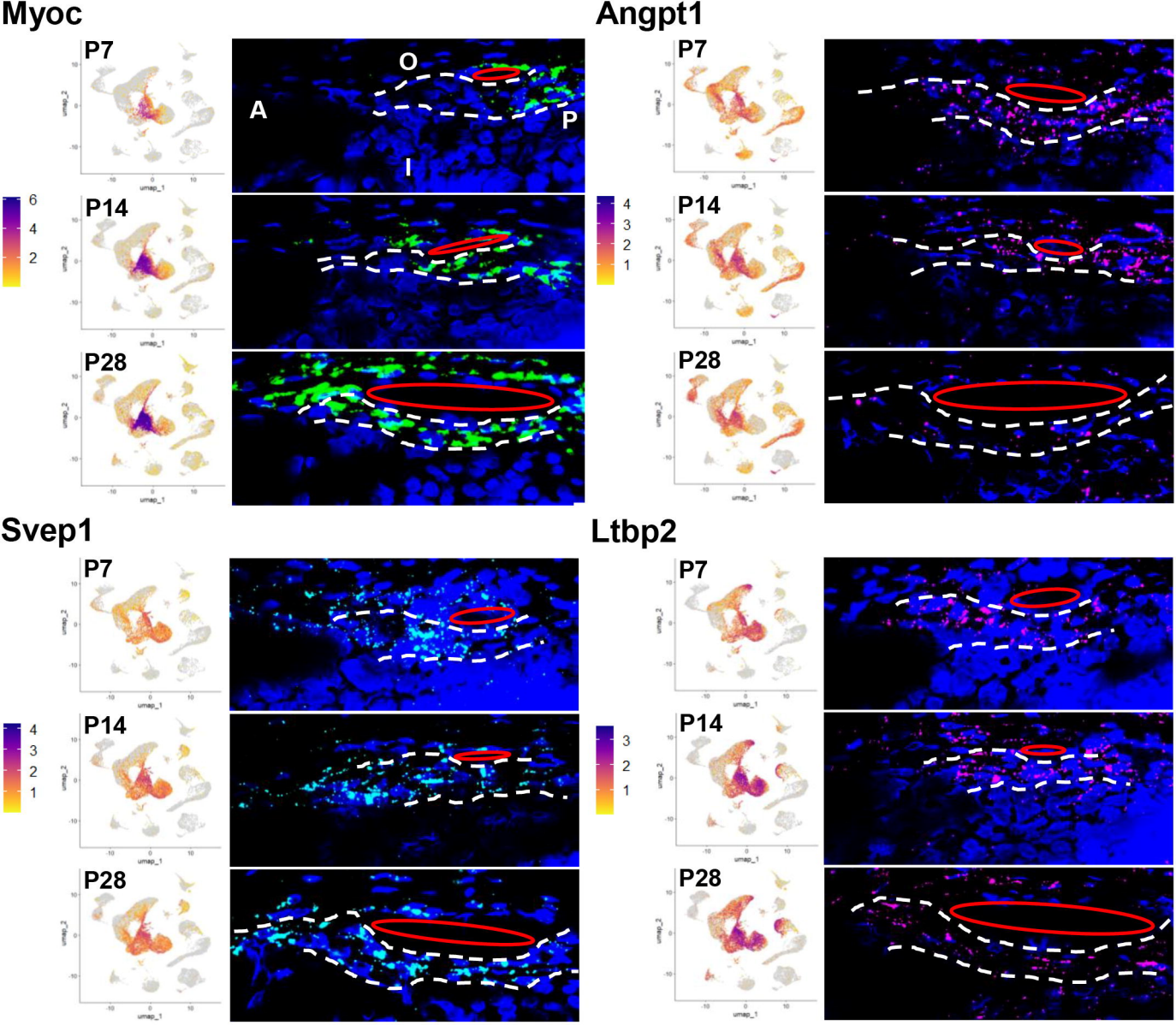
Myoc
Angpt1
Svep1
Ltbp2
P7
P14
P28
O
A
P
I
umap_1
umap_2

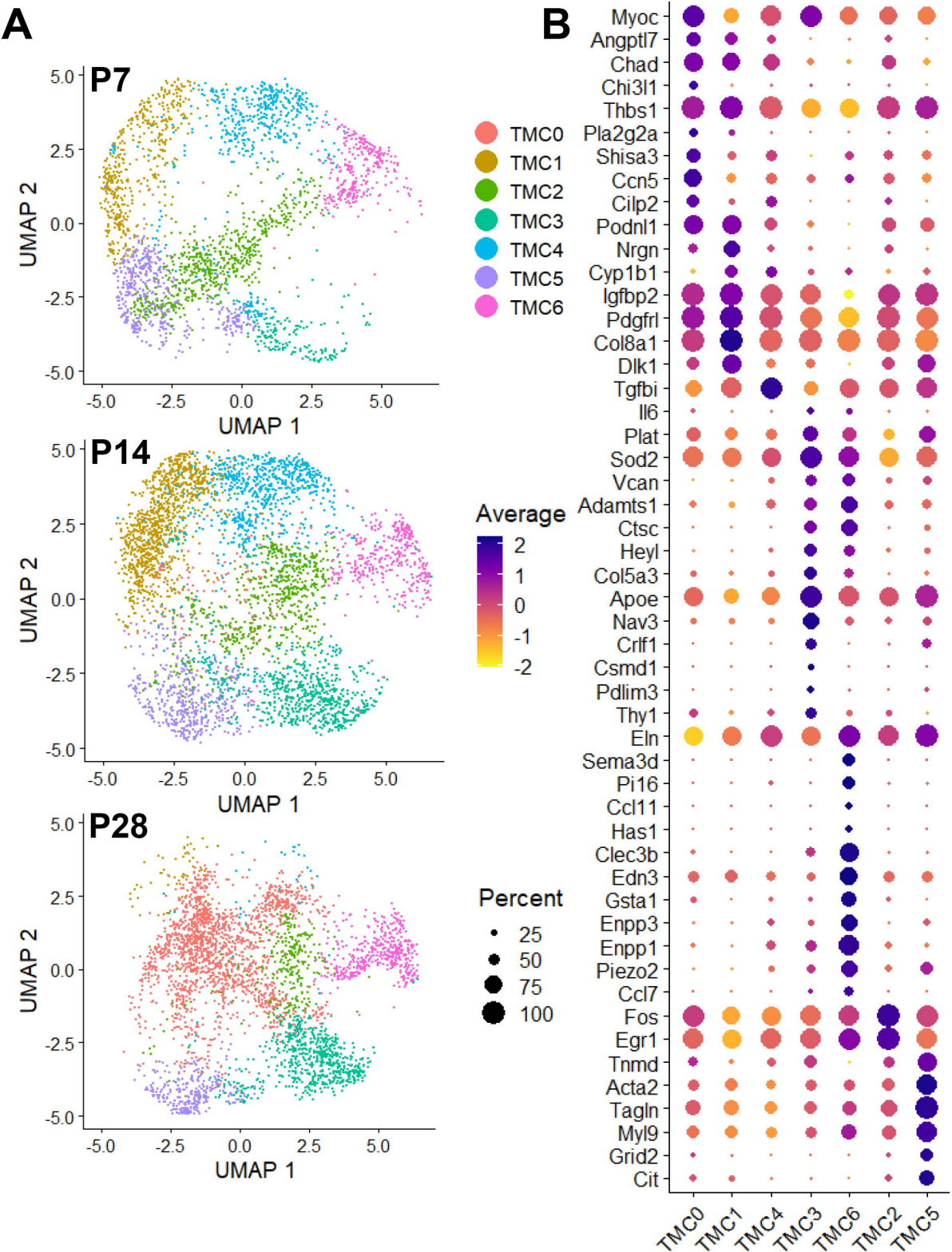
A
P7
P14
P28
UMAP 1
UMAP 2
5.0
2.5
0.0
-2.5
-5.0
TMC0
TMC1
TMC2
TMC3
TMC4
TMC5
TMC6
Average
2
1
0
-1
-2
Percent
25
50
75
100
B
Myoc
Angptl7
Chad
Chi3l1
Thbs1
Pla2g2a
Shisa3
Ccn5
Cilp2
Podnl1
Nrgn
Cyp1b1
Igfbp2
Pdgfrl
Col8a1
Dlk1
Tgfbi
Il6
Plat
Sod2
Vcan
Adamts1
Ctsc
Heyl
Col5a3
Apoe
Nav3
Crlf1
Csmd1
Pdlim3
Thy1
Eln
Sema3d
Pi16
Ccl11
Has1
Clec3b
Edn3
Gsta1
Enpp3
Enpp1
Piezo2
Ccl7
Fos
Egr1
Tnmd
Acta2
Tagln
Myl9
Grid2
Cit
TMC0
TMC1
TMC4
TMC3
TMC6
TMC2
TMC5

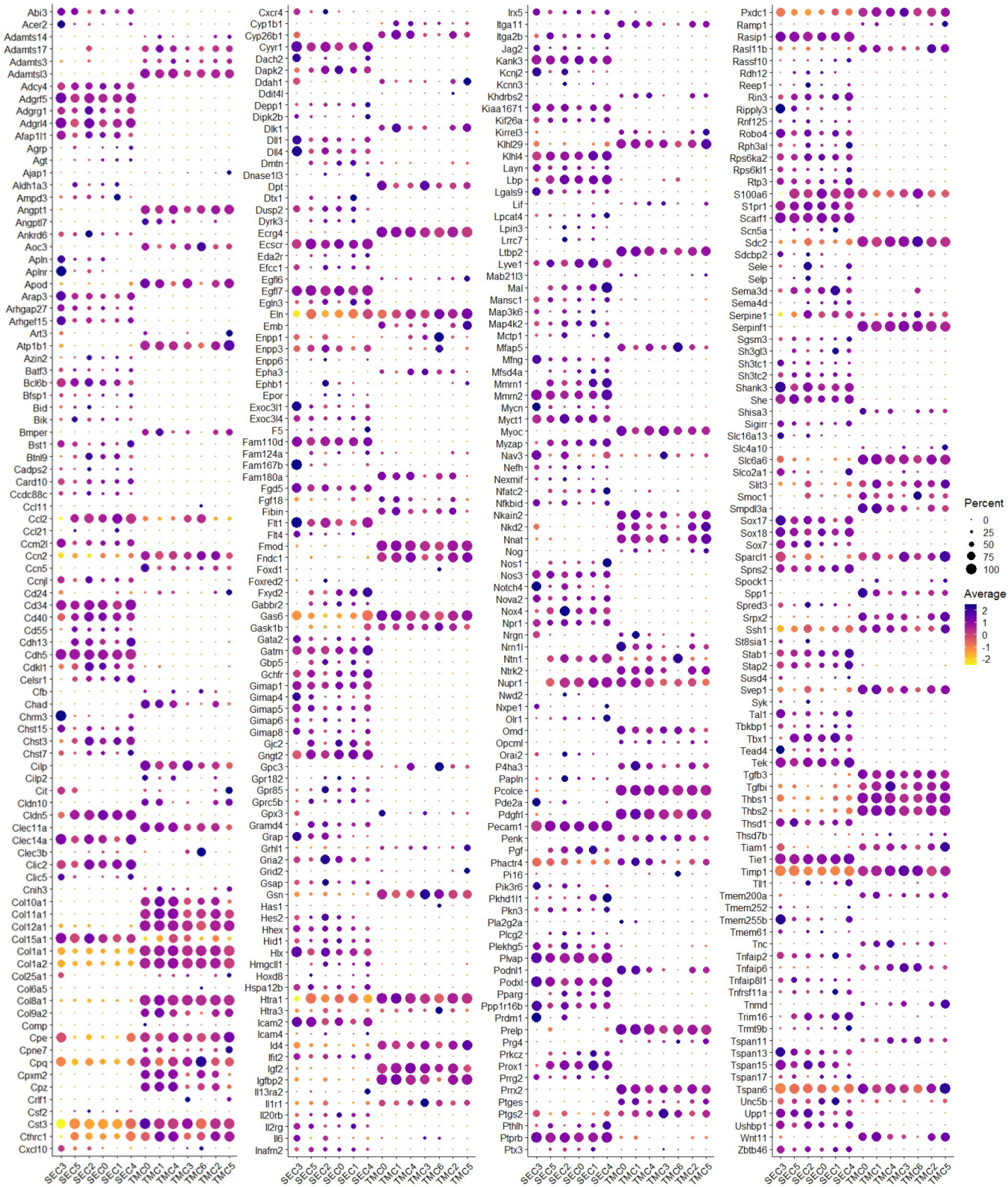
Abi3
Acer2
Adamts14
Adamts17
Adamts3
Adamtsl3
Adcy4
Adgrf5
Adgrg1
Adgrl4
Afap1l1
Agrp
Agt
Ajap1
Aldh1a3
Ampd3
Angpt1
Angptl7
Ankrd6
Aoc3
Apln
Aplnr
Apod
Arap3
Arhgap27
Arhgef15
Art3
Atp1b1
Azin2
Batf3
Bcl6b
Bfsp1
Bid
Bik
Bmper
Bst1
Btnl9
Cadps2
Card10
Ccdc88c
Ccl11
Ccl2
Ccl21
Ccm2l
Ccn2
Ccn5
Ccnjl
Cd24
Cd34
Cd40
Cd55
Cdh13
Cdh5
Cdkl1
Celsr1
Cfb
Chad
Chrm3
Chst15
Chst3
Chst7
Cilp
Cilp2
Cit
Cldn10
Cldn5
Clec11a
Clec14a
Clec3b
Clic2
Clic5
Cnih3
Col10a1
Col11a1
Col12a1
Col15a1
Col1a1
Col1a2
Col25a1
Col6a5
Col8a1
Col9a2
Comp
Cpe
Cpne7
Cpq
Cpxm2
Cpz
Crlf1
Csf2
Cst3
Cthrc1
Cxcl10
Cxcr4
Cyp1b1
Cyp26b1
Cyyr1
Dach2
Dapk2
Ddah1
Ddit4l
Depp1
Dipk2b
Dlk1
Dll1
Dll4
Dmtn
Dnase1l3
Dpt
Dtx1
Dusp2
Dyrk3
Ecrg4
Ecscr
Eda2r
Efcc1
Egfl6
Egfl7
Egln3
Eln
Emb
Enpp1
Enpp3
Enpp6
Epha3
Ephb1
Epor
Exoc3l1
Exoc3l4
F5
Fam110d
Fam124a
Fam167b
Fam180a
Fgd5
Fgf18
Fibin
Flt1
Flt4
Fmod
Fndc1
Foxd1
Foxred2
Fxyd2
Gabbr2
Gas6
Gask1b
Gata2
Gatm
Gbp5
Gchfr
Gimap1
Gimap4
Gimap5
Gimap6
Gimap8
Gjc2
Gngt2
Gpc3
Gpr182
Gpr85
Gprc5b
Gpx3
Gramd4
Grap
Grhl1
Gria2
Grid2
Gsap
Gsn
Has1
Hes2
Hhex
Hid1
Hlx
Hmgcll1
Hoxd8
Hspa12b
Htra1
Htra3
Icam2
Icam4
Id4
Ifit2
Igf2
Igfbp2
Il13ra2
Il1r1
Il20rb
Il2rg
Il6
Inafm2
Irx5
Itga11
Itga2b
Jag2
Kank3
Kcnj2
Kcnn3
Khdrbs2
Kiaa1671
Kif26a
Kirrel3
Klhl29
Klhl4
Layn
Lbp
Lgals9
Lif
Lpcat4
Lpin3
Lrrc7
Ltbp2
Lyve1
Mab21l3
Mal
Mansc1
Map3k6
Map4k2
Mctp1
Mfap5
Mfng
Mfsd4a
Mmrn1
Mmrn2
Mycn
Myct1
Myoc
Myzap
Nav3
Nefh
Nexmif
Nfatc2
Nfkbid
Nkain2
Nkd2
Nnat
Nog
Nos1
Nos3
Notch4
Nova2
Nox4
Npr1
Nrgn
Nrn1l
Ntn1
Ntrk2
Nupr1
Nwd2
Nxpe1
Olr1
Omd
Opcml
Orai2
P4ha3
Papln
Pcolce
Pde2a
Pdgfrl
Pecam1
Penk
Pgf
Phactr4
Pi16
Pik3r6
Pkhd1l1
Pkn3
Pla2g2a
Plcg2
Plekhg5
Plvap
Podnl1
Podxl
Pparg
Ppp1r16b
Prdm1
Prelp
Prg4
Prkcz
Prox1
Prrg2
Prrx2
Ptges
Ptgs2
Pthlh
Ptprb
Ptx3
Pxdc1
Ramp1
Rasip1
Rasl11b
Rassf10
Rdh12
Reep1
Rin3
Ripply3
Rnf125
Robo4
Rph3al
Rps6ka2
Rps6kl1
Rtp3
S100a6
S1pr1
Scarf1
Scn5a
Sdc2
Sdcbp2
Sele
Selp
Sema3d
Sema4d
Serpine1
Serpinf1
Sgsm3
Sh3gl3
Sh3tc1
Sh3tc2
Shank3
She
Shisa3
Sigirr
Slc16a13
Slc4a10
Slc6a6
Slco2a1
Slit3
Smoc1
Smpdl3a
Sox17
Sox18
Sox7
Sparcl1
Spns2
Spock1
Spp1
Spred3
Srpx2
Ssh1
St8sia1
Stab1
Stap2
Susd4
Svep1
Syk
Tal1
Tbkbp1
Tbx1
Tead4
Tek
Tgfb3
Tgfbi
Thbs1
Thbs2
Thsd1
Thsd7b
Tiam1
Tie1
Timp1
Tll1
Tmem200a
Tmem252
Tmem255b
Tmem61
Tnc
Tnfaip2
Tnfaip6
Tnfaip8l1
Tnfrsf11a
Tnmd
Trim16
Trmt9b
Tspan11
Tspan13
Tspan15
Tspan17
Tspan6
Unc5b
Upp1
Ushbp1
Wnt11
Zbtb46
SEC3
SEC5
SEC2
SEC0
SEC1
SEC4
TMC0
TMC1
TMC4
TMC3
TMC6
TMC2
TMC5
Percent
0
25
50
75
100
Average
2
1
0
-1
-2

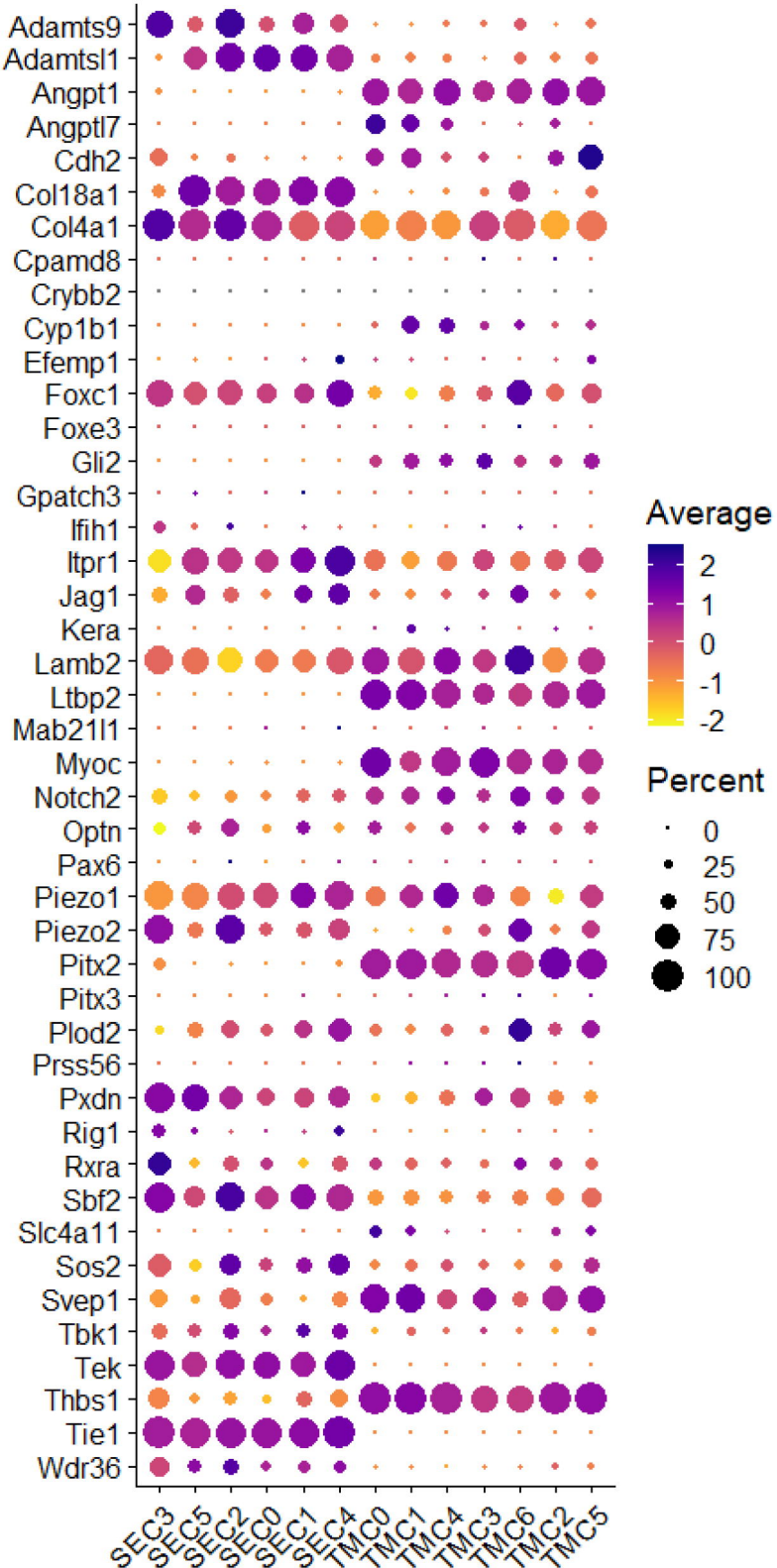
Adamts9
Adamtsl1
Angpt1
Angptl7
Cdh2
Col18a1
Col4a1
Cpamd8
Crybb2
Cyp1b1
Efemp1
Foxc1
Foxe3
Gli2
Gpatch3
Ifih1
Itpr1
Jag1
Kera
Lamb2
Ltbp2
Mab21l1
Myoc
Notch2
Optn
Pax6
Piezo1
Piezo2
Pitx2
Pitx3
Plod2
Prss56
Pxdn
Rig1
Rxra
Sbf2
Slc4a11
Sos2
Svep1
Tbk1
Tek
Thbs1
Tie1
Wdr36
SEC3
SEC5
SEC2
SEC0
SEC1
SEC4
TMC0
TMC1
TMC4
TMC3
TMC6
TMC2
TMC5
Average
2
1
0
-1
-2
Percent
0
25
50
75
100